In-Situ Synchrotron X-Ray Diffraction Experiments for Validation of Numerical Models of Microstructural Evolution in Welds

by: John W. Elmer, Lawrence Livermore National Laboratory

Lawrence Livermore National Laboratory

Prepared for:

2015 Workshop on Collection and Analysis of Big Data in 3D Materials Science

May 12-14, 2014,

UCSB, Santa Barbara, CA, USA
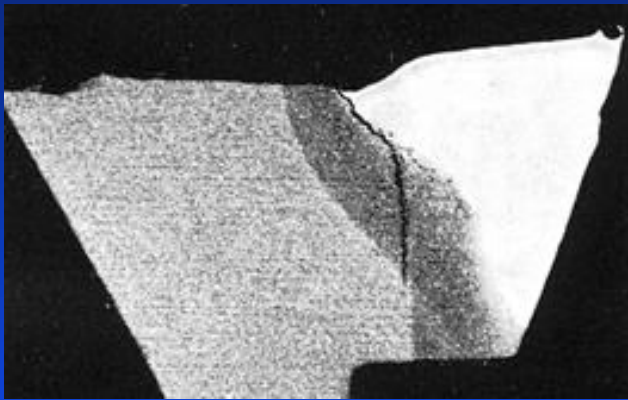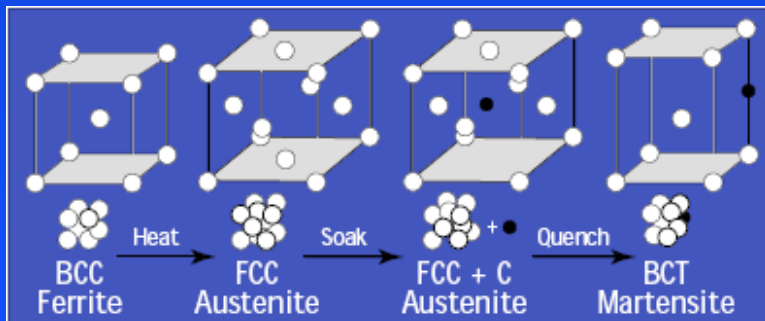
Welding creates microstructural changes that alter the properties of the, otherwise good, base metals that they join

Low toughness in steel welds caused by the formation of martensite has resulted in some spectacular failures

Failure in welded steel HAZ

BCC Ferrite → Heat → FCC Austenite → Soak → FCC + C Austenite → Quench → BCT Martensite

Liberty ship failures were attributed to:
- all-welded construction
- welds in materials with low toughness
- presence of flaws in welded joints

Fracture mechanics just beginning to develop

Microstructural evolution in welds occurs under highly non-isothermal conditions, producing macro- and microstructural gradients

In titanium (below), heating, solidification, $\alpha \rightarrow \beta \rightarrow \alpha$ phase transformations, and grain growth all combine to create the final weld microstructure

Base   Metal   HAZ-1   HAZ-2   Fusion Zone

CP Titanium
Arc Weld

a   b   c   d

1 mm
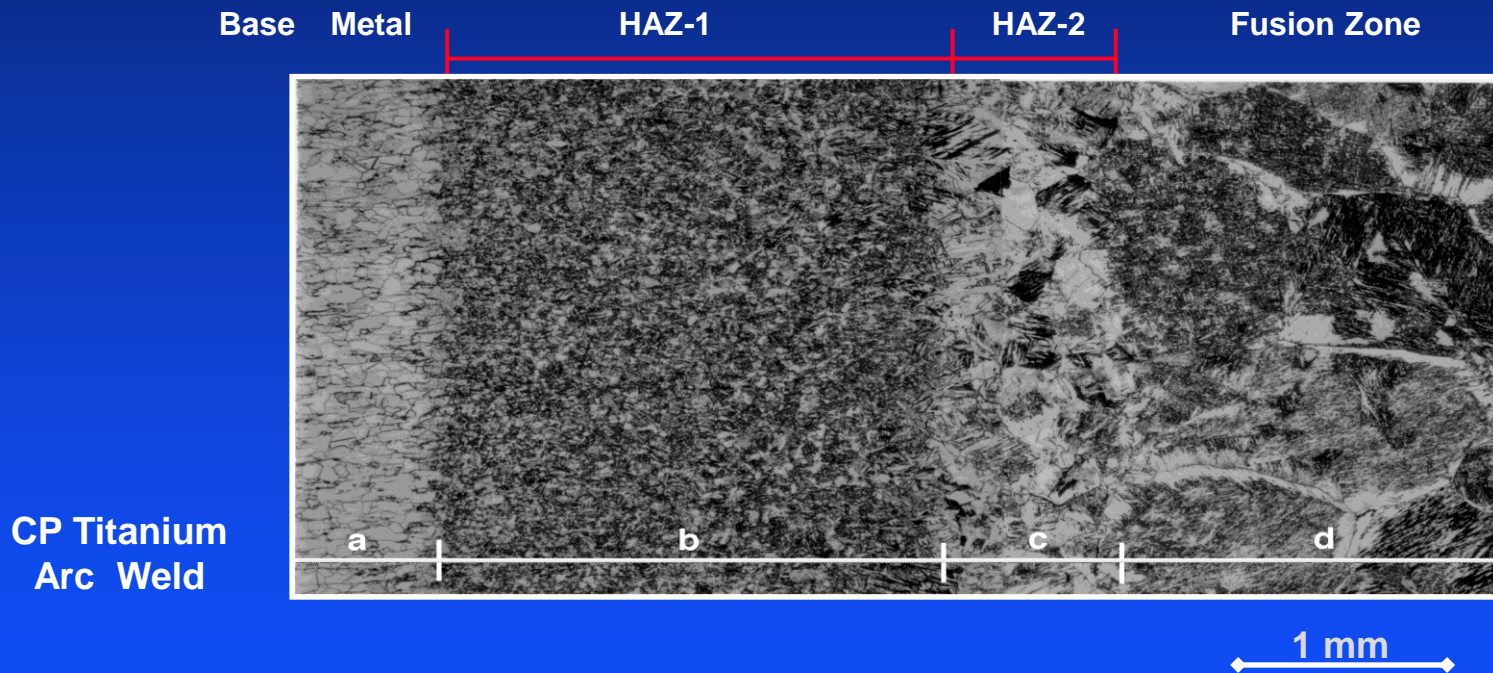
An in-situ X-Ray "probe" would allow us to visualize how the crystal structure evolves in real time, instead of just a microstructural "snapshot" after the weld is completed
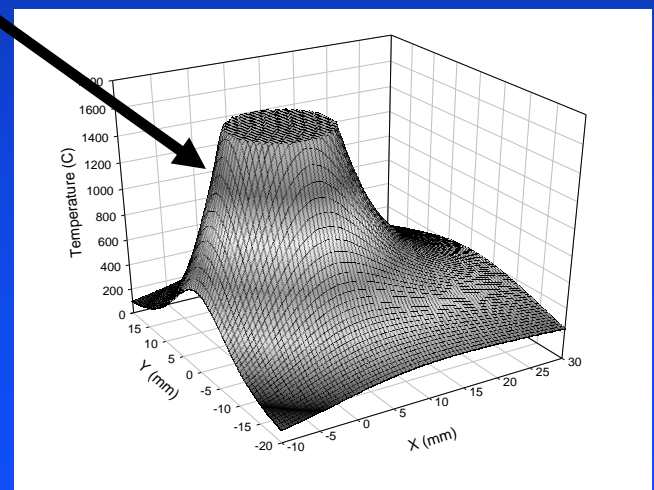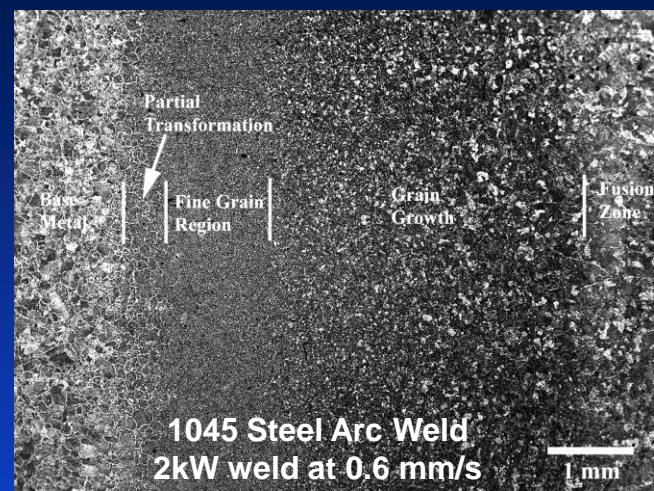
Direct observation of phase transformations during welding would require small probe sizes

Microstructural gradients in the HAZ of arc welds are typically only a few millimeters wide

Temperature gradients are ~10^2 K/mm for most arc welds, and higher for laser and electron beam welds

> **Sub-mm non-contact probes are required**

Synchrotron radiation is the key for creating a small non-contact X-Ray "probe" !

1045 Steel Arc Weld
2kW weld at 0.6 mm/s

Partial Transformation

Base Metal | Fine Grain Region | Grain Growth | Fusion Zone

1 mm

Temperature Fields Produced by Traveling Distributed Heat Source
T.W. Eagar and N-S Tsai
Welding Journal, Dec, 1983

$$T(x,y,z,P,v,\sigma,t)=T_O+\left(\frac{\eta P}{\pi\rho c\sqrt{4\pi\alpha}}\right)*\int_0^t\left\{\left(\frac{1}{2\alpha t3/2+\sigma^2 t1/2}\right)\exp\left(\left(\frac{-(x-vt)^2+y^2}{4\alpha t+2\sigma^2}\right)-\left(\frac{z^2}{4\alpha t}\right)\right)\right\}dt$$

Synchrotron radiation provides a high flux, low divergence, tunable x-ray beam for in-situ experiments

In-Situ welding experiments were performed at SSRL

The Stanford Synchrotron Radiation
Laboratory (SSRL),
Palo Alto, California.

Commissioned 1973, 3GeV (2nd gen)
Upgraded in 2004-2006

**Controlled heating/cooling experiments to simulate welds at APS**

The Advanced Photon Source (APS).
Located at Argonne National Laboratory,
near Chicago, Illinois

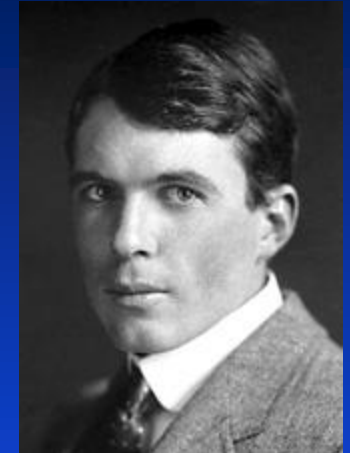Commissioned 1997 , 7 GeV (3rd gen)

It's been 100 years since Bragg(s) discovered XRD: "The analysis of crystal structure by means of X-rays"

Bragg's analysis of x-ray diffraction opened up the field of crystallography, allowing us to understand how the atoms are positioned relative to each other in a crystal.
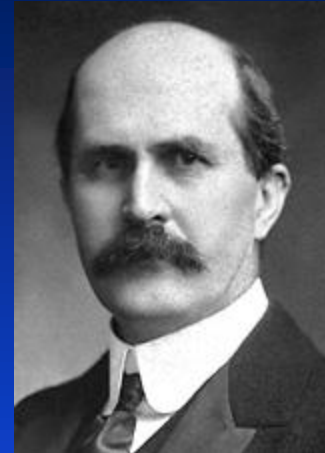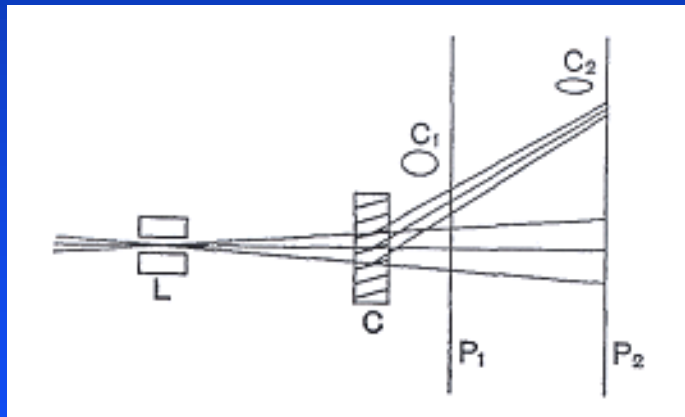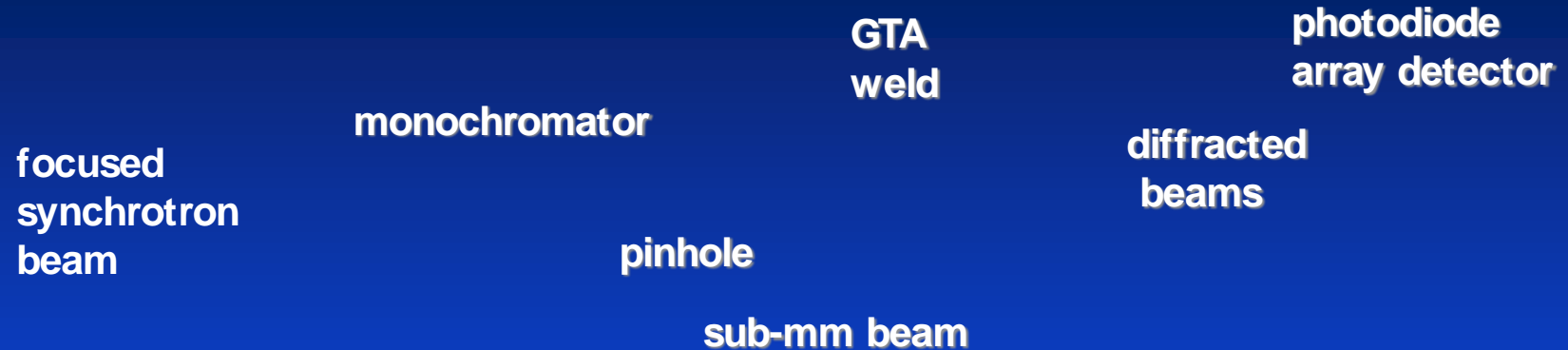

Sir W. H. Bragg
1862-1942

W. L. Bragg
1890-1971

Bragg's Equation

$$n \lambda = 2\, d\, \sin(\theta)$$

Bragg, 1912 analysis of Laue's spots, Received Nobel Prize in 1915

# Synchrotron-based X-ray diffraction setup for in-situ investigations of transformations during welding at SSRL

GTA weld

photodiode array detector

monochromator

focused synchrotron beam

diffracted beams

pinhole

sub-mm beam

- 31 pole wiggler at SSRL
- 8 to 12 keV beam
- 2.3 mrad divergence
- 180-540 μm pinhole
- ~10^{10} photons/s
- 2" Si photodiode array detector for a 2θ range of 30°

cylindrical sample

Two synchrotron-based experiments were developed by LLNL for in-situ weld observations
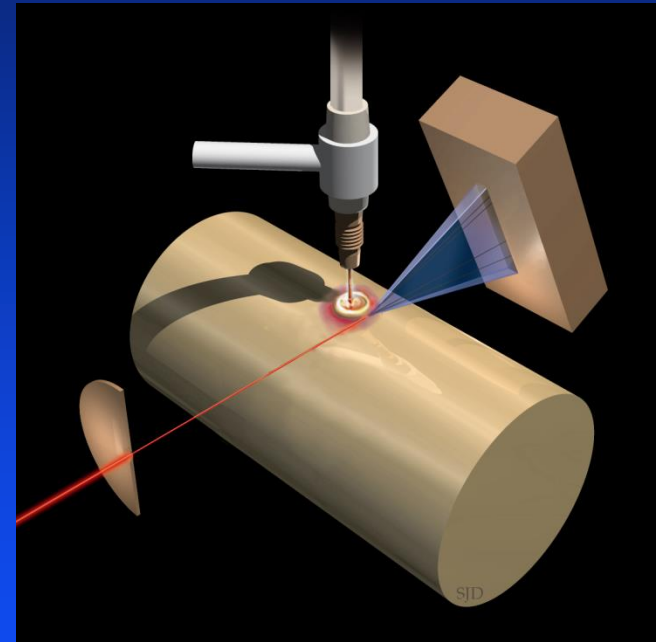
## Spatially Resolved X-Ray Diffraction (SRXRD) is used for phase mapping
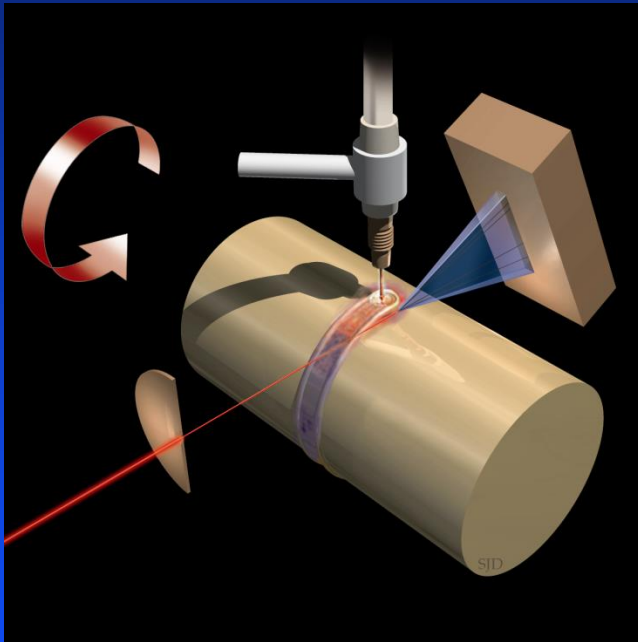
- Bar rotates at constant speed
- Steady state weld established
- Weld is jogged wrt X-ray beam

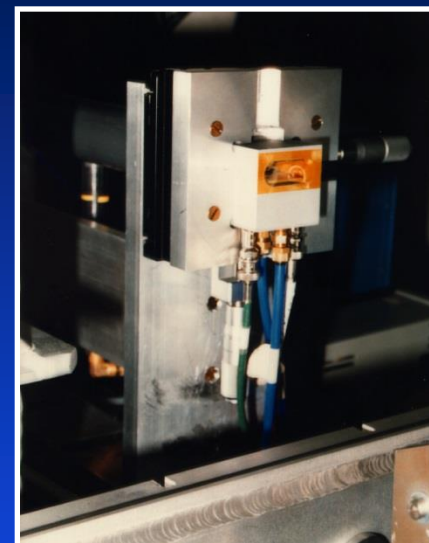## Time Resolved X-Ray Diffraction (TRXRD) is used for phase dynamics

- Stationary bar and X-ray position
- Transient heating/cooling spot weld
- 600 diffraction patterns in 30 seconds

SRXRD environmental enclosure for inert gas welding in helium with IR imaging of weld pool
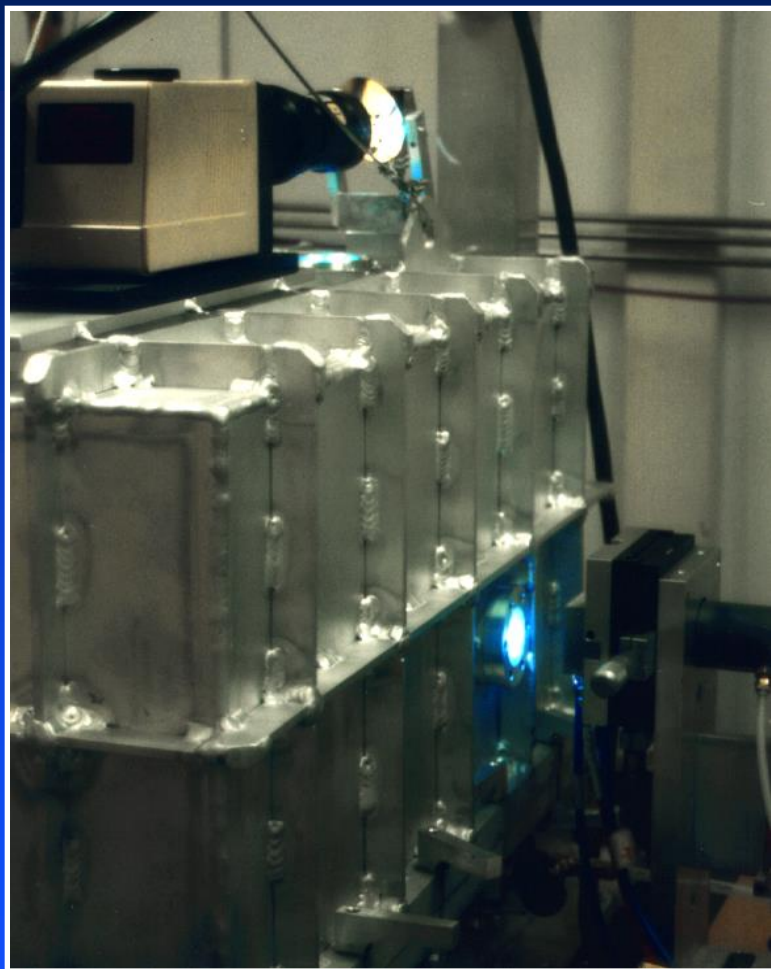
welding stage

beam line and pinhole

experiment in progress

In-situ weld observations require sub-millimeter non-contact probes with high spatial resolution

Infrared image taken during arc welding

Extreme *in-situ* conditions are present during welding

- ➤ High peak temperatures
  exceed the melting point of weld metal
- ➤ Welding arc
  >20,000 deg., intense UV and IR
- ➤ Weld fumes and soot
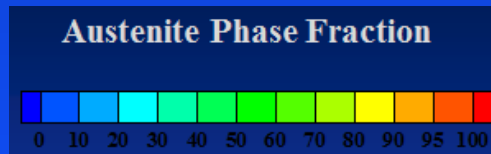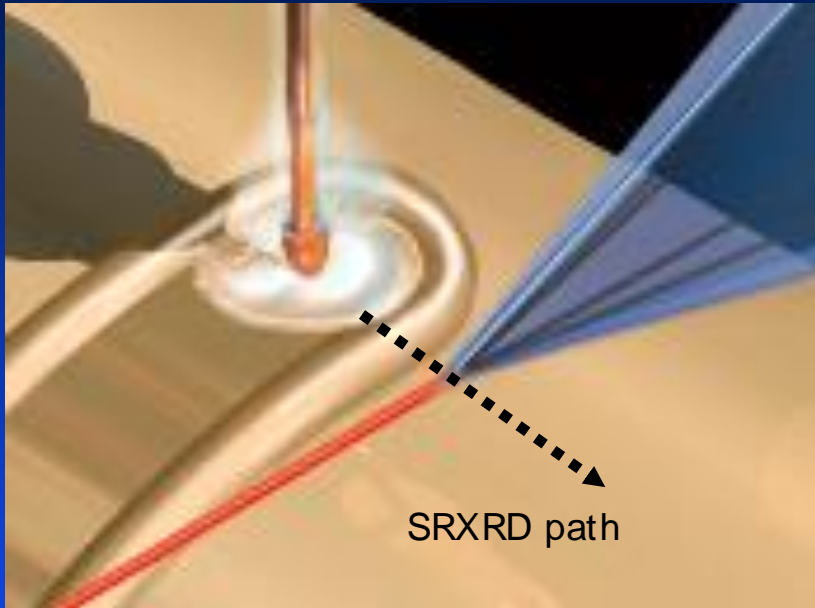- ➤ Temperature gradients
  on the order of 10^2 K/mm

A sub-mm, non-contact probe is required for in-situ investigations of welds
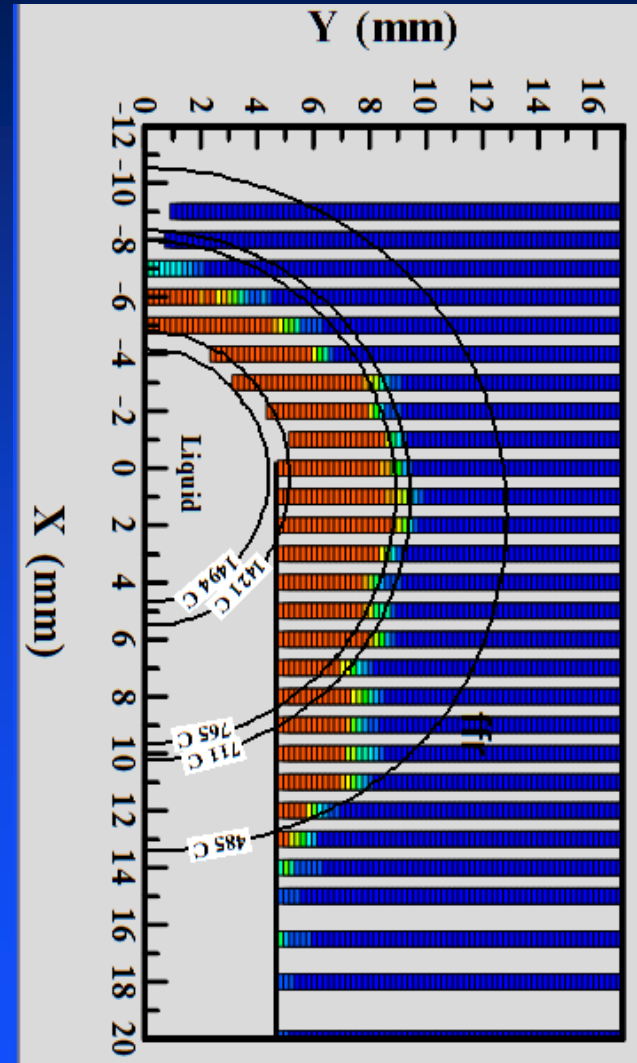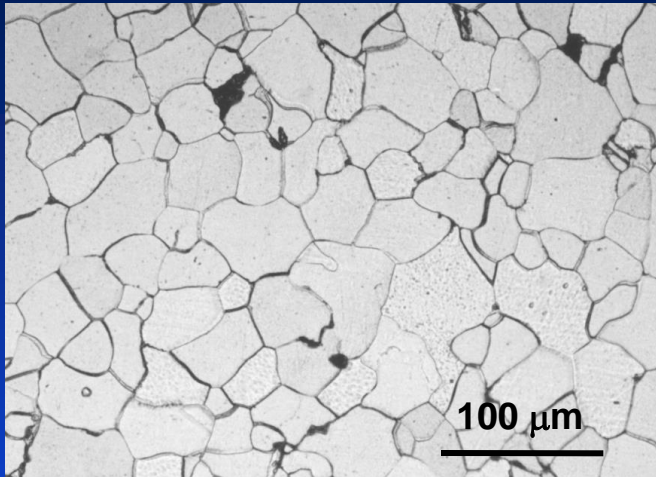
10 mm

Part I
Spatially Resolved X-Ray Diffraction (SRXRD)

SRXRD path

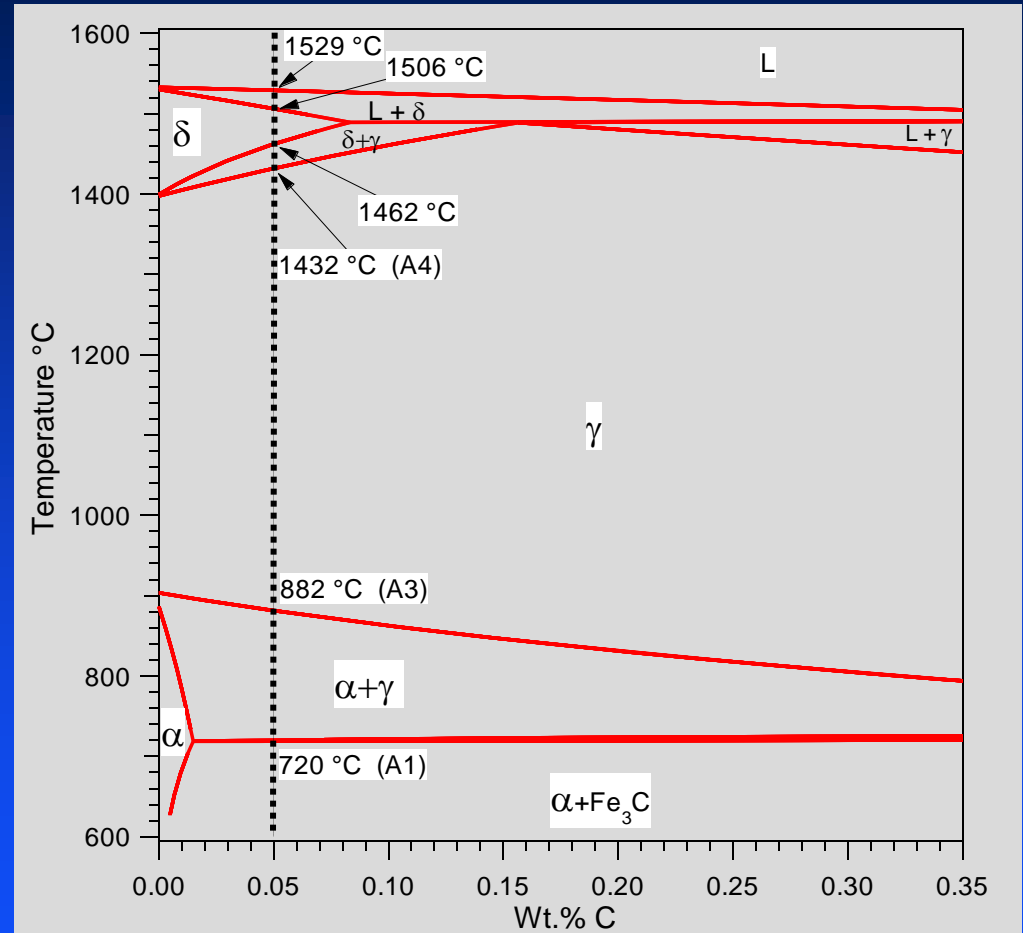**Austenite Phase Fraction**

0 10 20 30 40 50 60 70 80 90 95 100

Phase map surrounding a
1045 steel arc weld (2kW at 6 mm/s)
as measured using SRXRD

AISI 1005 carbon-manganese steel has three allotropic phases α (bcc), γ (fcc), δ (bcc)
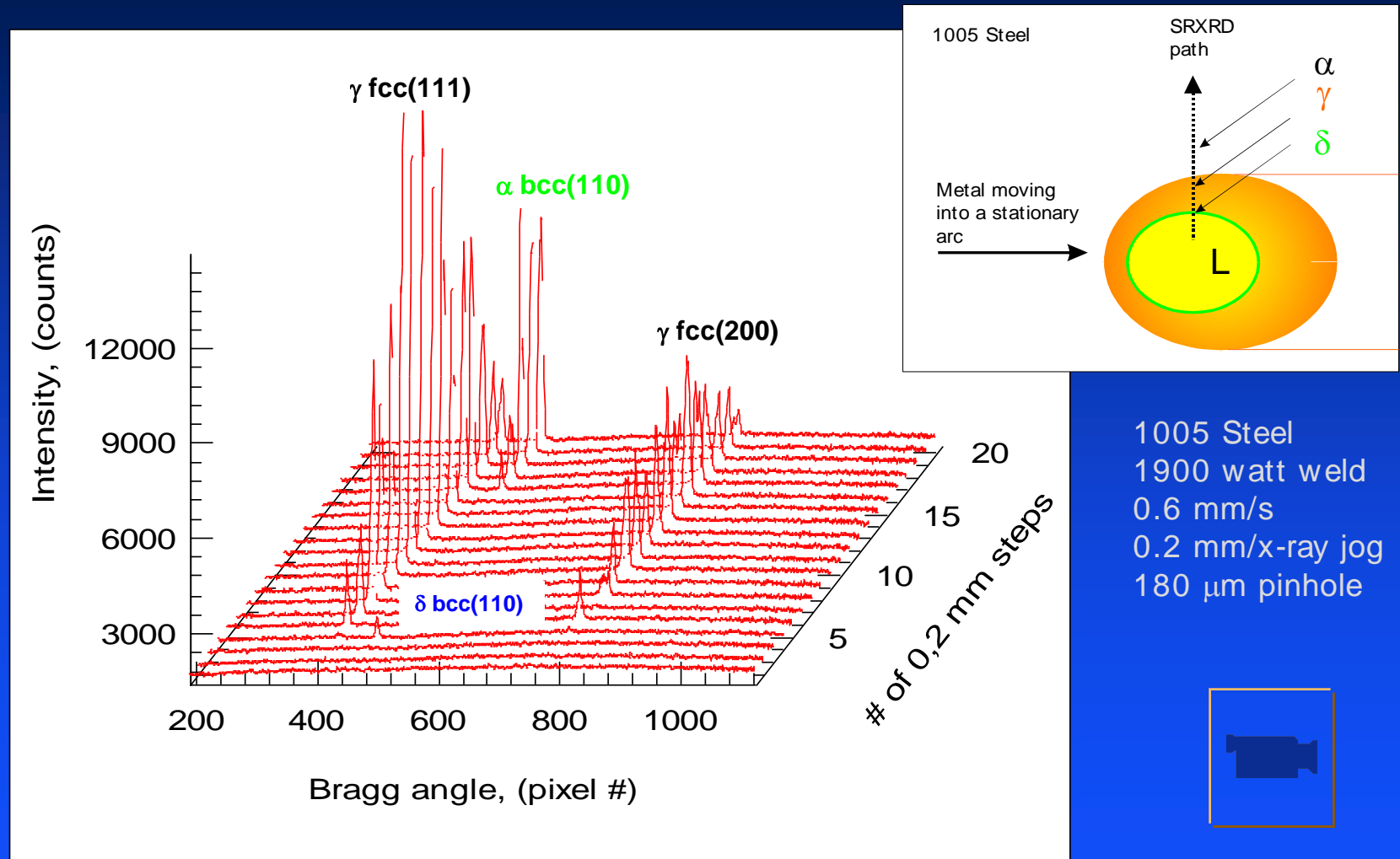

100 μm

The as received microstructure shows equiaxed grains with occasional pearlite at grain boundaries

Fe, 0.05 C, 0.31 Mn, 0.18 Si, <0.005 Al (wt%)

Phase mapping is performed in rows of data, starting from the centerline of the weld

1005 Steel
1900 watt weld
0.6 mm/s
0.2 mm/x-ray jog
180 μm pinhole

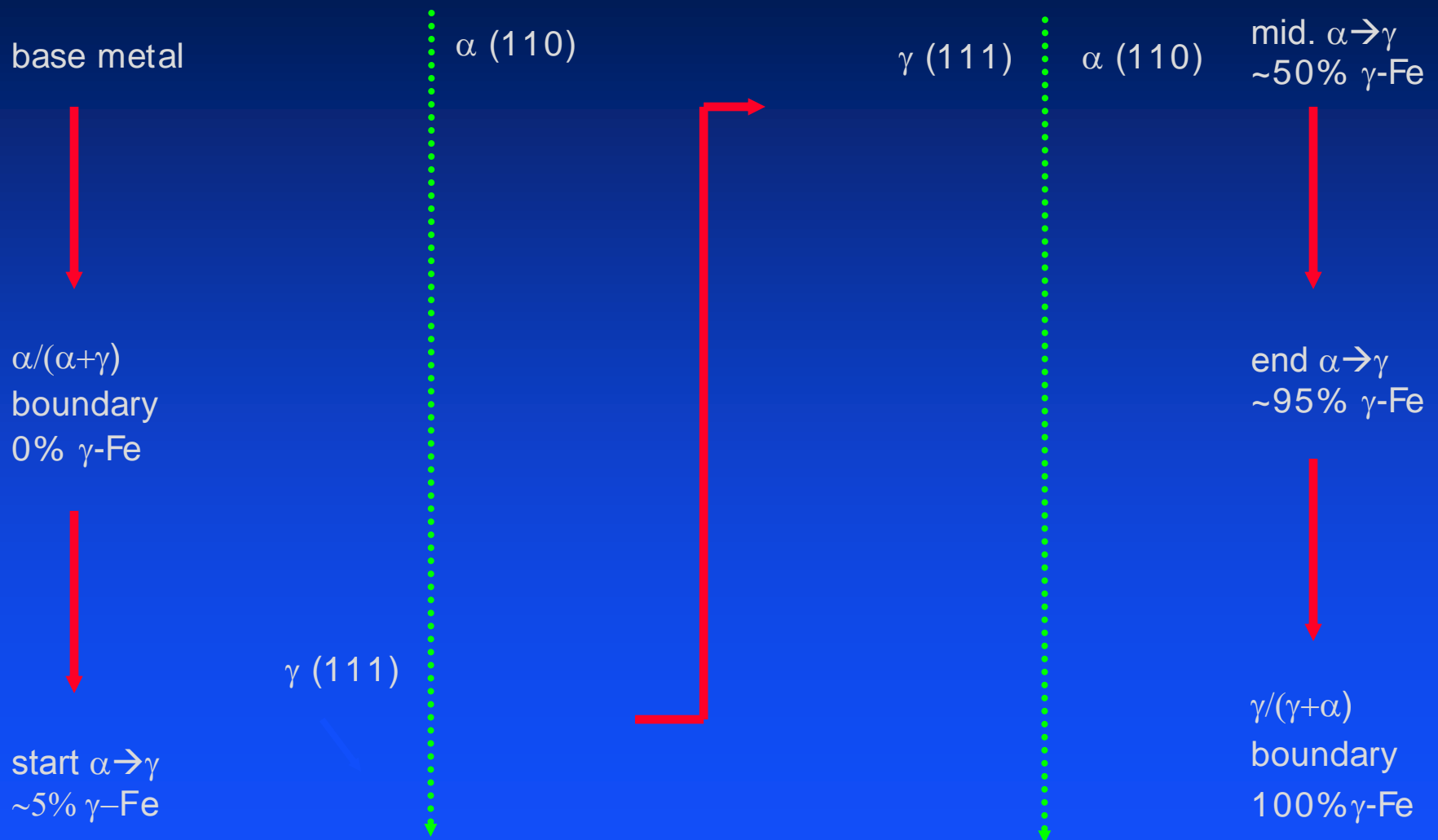# *The high-temperature δ-Fe phase in C-Mn steel was directly observed for the first time using SRXRD*

The presence of δ-ferrite at the liquid pool boundary allows for epitaxial regrowth of δ-ferrite during solidification

Starting from the liquid, δ-Fe was first observed adjacent to the weld pool, followed by the transformation to γ-Fe at intermediate temperatures, then followed by the transformation to α-Fe at low temperatures
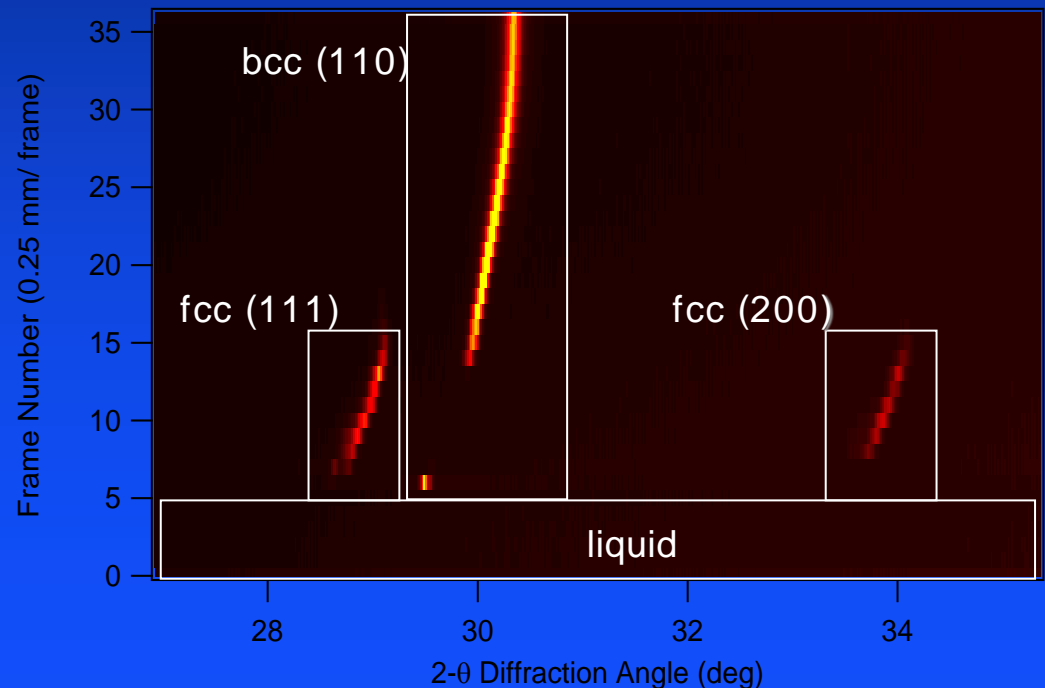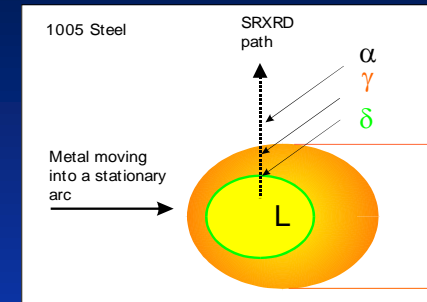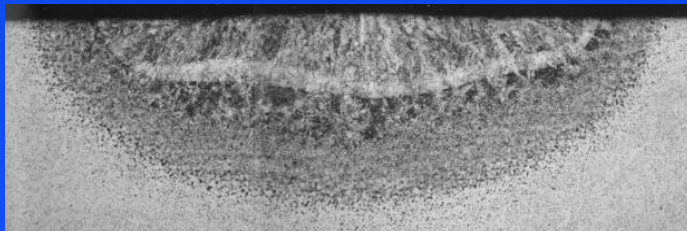
The x-ray diffraction peaks contain quantitative information about the relative fraction of α-Fe and γ-Fe

base metal

α (110)

γ (111) α (110)

mid. $\alpha \rightarrow \gamma$
~50% γ-Fe

$\alpha/(\alpha+\gamma)$
boundary
0% γ-Fe

end $\alpha \rightarrow \gamma$
~95% γ-Fe

γ (111)

start $\alpha \rightarrow \gamma$
~5% γ–Fe

$\gamma/(\gamma+\alpha)$
boundary
100% γ-Fe

The x-ray peak areas are converted into relative volume fractions of the α and γ phases

Contributing factors:

- **Integrated peak areas (measured intensities) are scaled to account for the symmetry of the target crystal structure, the geometry of the experiment, and thermal effects**

- **The scaled intensities represent the relative contributions of the integrated areas to the phase volume fractions**

- **Volume fractions are determined by finding the ratio of the scaled peak intensities for a given phase to the total scaled intensity of all peaks**

- *Structure factor:*

  where $f =$ atomic scattering factor

- *Multiplicity: $p =$* # permutations of $\pm h$, $\pm k$, $\pm l$ contributing to same reflection

- *Lorentz-polarization (geometric) factor:*
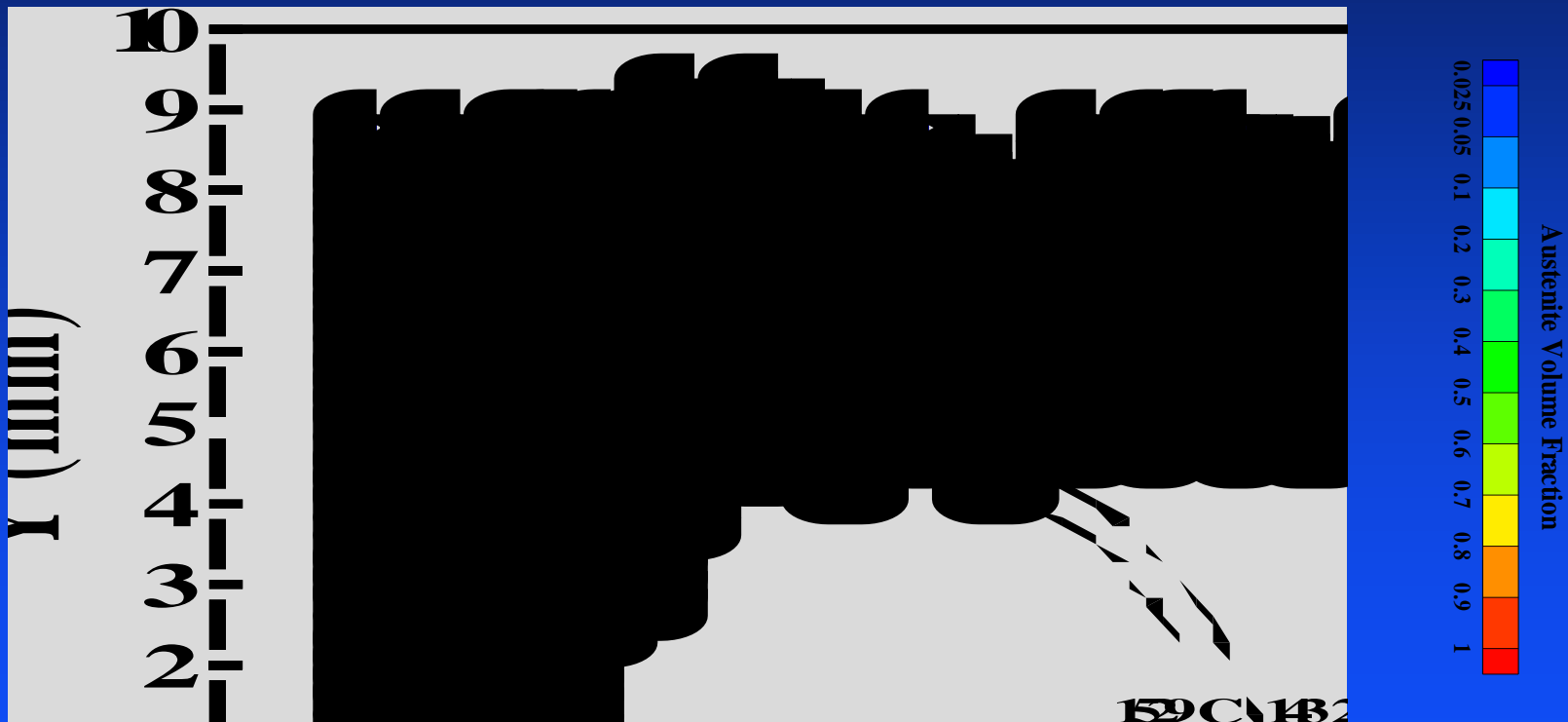
- *Temperature factor:*

  where:

  $\Theta =$ Debye temperature,

The SRXRD patterns were further analyzed to create a phase map of the weld HAZ in 1005 steel

The diffraction peaks were fit with a Gaussian profile, then peak areas were then converted into volume fraction of the respective phases

J. W. Elmer, Joe Wong and Thorsten Ressler, "Spatially Resolved X-Ray Diffraction Mapping of Phase Transformations in the HAZ of Carbon-Manganese Steel Arc Welds," Metall. and Mater. Trans. A, 32A (5), pp. 1175-1187, 2001.

3D coupled thermal-fluids numerical modeling is used for a more realistic prediction of weld temperatures

Equations for conservation of mass, momentum, and energy are solved in a moving coordinate system.
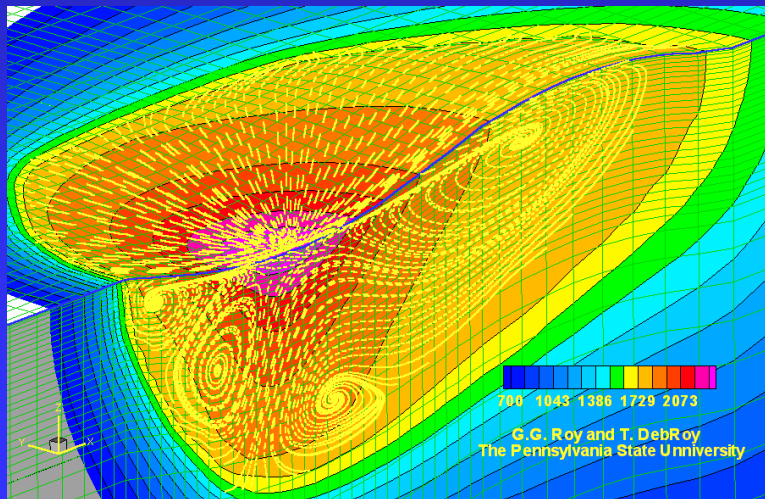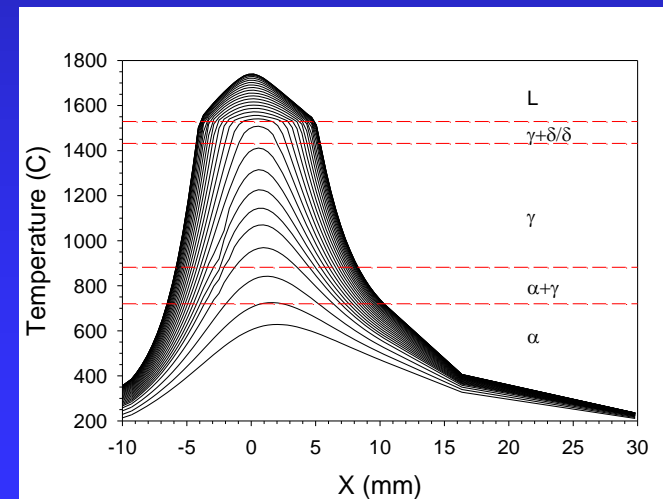
Energy:

Momentum:

Continuity :

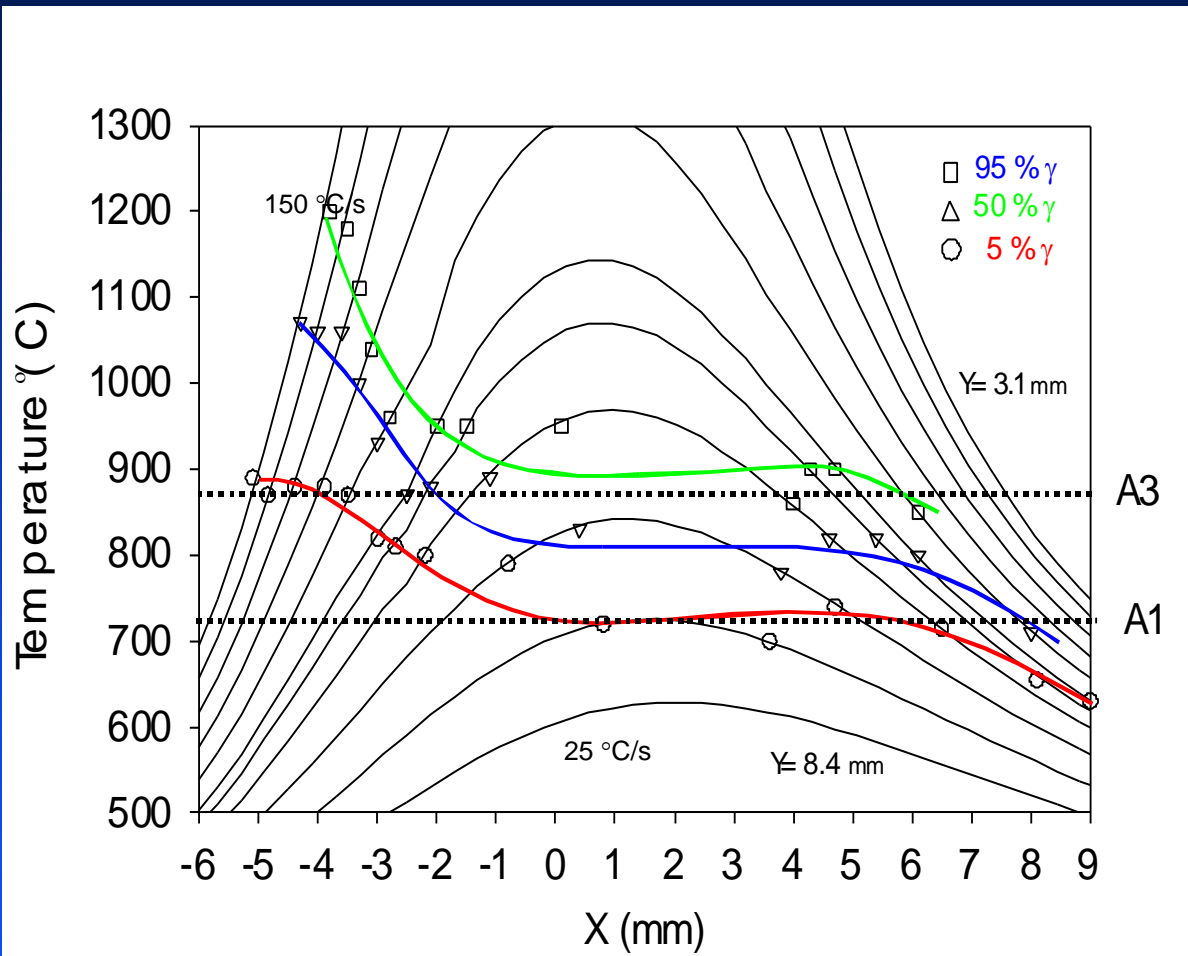G.G. Roy and T. DebRoy
The Pennsylvania State Unniversity

Professor DebRoy, Penn State University

Thermal profiles parallel to weld direction in steel

SRXRD results, combined with the thermal model, map the important kinetics for α→γ→α transformation in the weld

The final plot gives lines of constant transformation, showing the start (5%), middle (50%), and completion (95%) of the ferrite/austenite transformation under the entire range of HAZ heating and cooling rates.

J. W. Elmer, T. A. Palmer, W. Zhang, B. Wood, and T. DebRoy, "Kinetic Modeling of Phase Transformations Occurring in the HAZ of C-Mn Steel Welds Based on Direct Observations," Acta Materialia, V51, pp. 3333-3349, 2003.

The Johnson-Mehl-Avrami kinetic model was used to fit the solid state phase transformations

JMA models the effects of time and temperature on the fraction transformed

$$f = 1 - \exp[-\{k_0 \exp(\frac{-Q}{RT})t\}^n]$$

Sigmoidal transformation Kinetics *

JMA Assumptions
- random, time dependent, volumetric nucleation
- spherical particle growth
- nucleation and growth effects combined together
- isothermal conditions

Question: what values of <u>Q, n, and ko </u>are reasonable ?

- with three unknown parameters, there are many combinations of them that will fit the experimental data

* Avrami, M , "Kinetics of Phase Change. I. General Theory". *Journal of Chemical Physics* **7** (12): 1103–1112, 1939.

The JMA relationship was modified for non-isothermal behavior of welds, and applied to 1005 steel

Wei Zhang et al.

$$f = 1 - \exp[-\{\sum_{i=1}^{m} k_0 \times \exp(-\frac{Q}{RT_i}) \times \Delta t\}^n]$$

$$\ln\{-\ln(1-f)\} = n \ln s + n \ln k_0$$

$$s = \sum_{i=1}^{m} \Delta t \times \exp(-\frac{Q}{RT_i})$$

F = fraction γ transformed
Δt = time step
Q = activation energy $\alpha \rightarrow \gamma$
n = JMA exponent
k_0 = pre-exponential constant
R = universal gas constant
Ti = temperature at ith time step

W. Zhang, J. W. Elmer, and T. DebRoy, "Kinetics of Ferrite to Austenite Phase Transformation during Welding of 1005 Steel," *Scripta Materialia*, 46, pp753-757, 2002.

Calculated JMA parameters

n = 1.62 ± 0.10
ln (k_0) = 11.63 ± 1.4

Q = 117.07 kJ/mol,
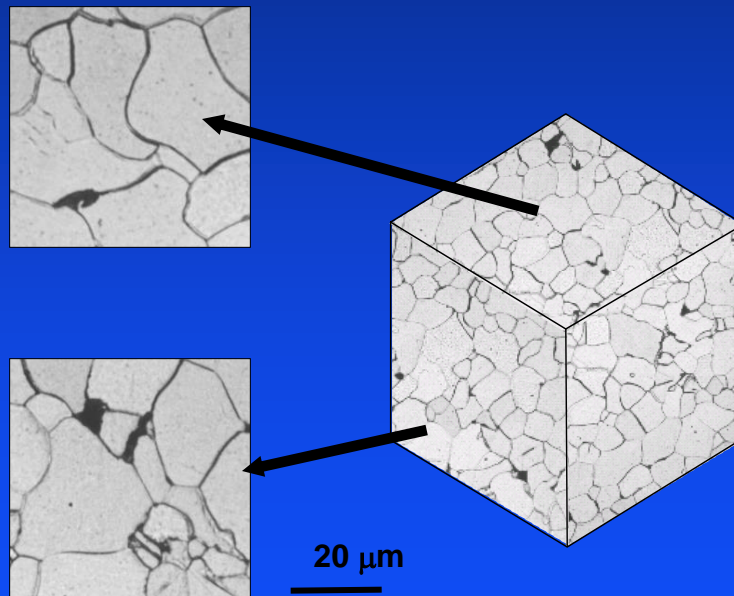~for carbon diffusion
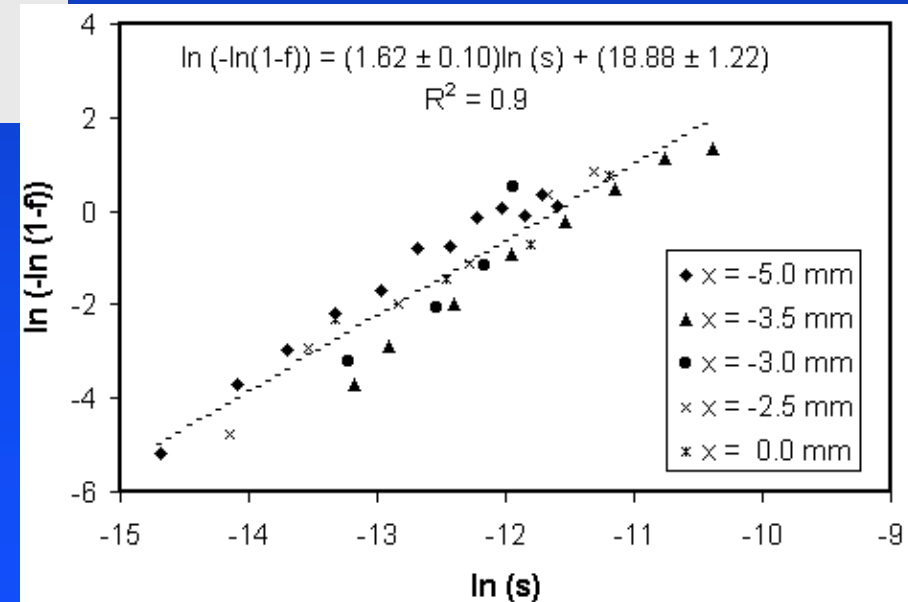
Before modeling, gain as much information about the phase transformation by examining the microstructural clues
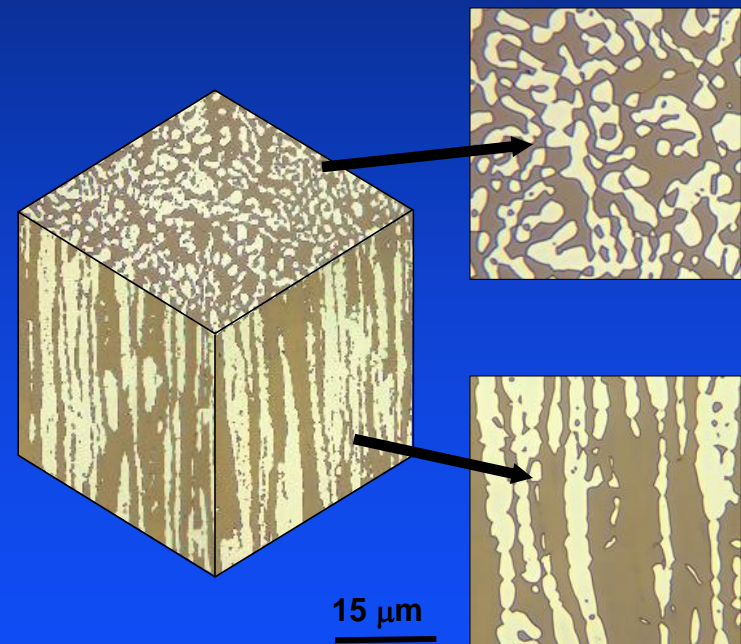
AISI 1005 steel

- **Nucleation first from pearlitic regions**
  - **number density can be measured**
- **Equiaxed microstructure**
  - **grain size can be measured**

20 μm

2205 Duplex Stainless Steel

- **Nucleation not required**
- **Grain texture plays a role**
  - **'spherical' growth invalid**

15 μm

W. Zhang, J. W. Elmer, and T. Debroy, "Integrated Modeling of Thermal Cycles, austenite formation, grain growth and decomposition in the heat affected zone of carbon steel," Science and Technology of Welding and Joining, V10(5), pp 574-582, 2005.

W. Zhang, T., DebRoy, T. A. Palmer, and J. W. Elmer, "Modeling of Ferrite Formation in a Duplex Stainless Steel Weld Considering Non-uniform Starting Microstructure," Acta Materialia, V53, p. 4441, 2005

JMA can be rewritten to incorporate separate nucleation and growth components, but problems exist here as well

JMA can be rewritten to incorporate separate N&G effects

- 1D, 2D and 3-D models have been derived *

$$f = 1 - \exp[(-\pi/3)\{k_n \exp(\frac{-Q_n}{RT})\}\{k_g \exp(\frac{-Q_g}{RT})\}^3 t^4]$$

3-D model

Assumptions
- volumetric, time dependent, nucleation
- spherical particle growth
- isothermal conditions

Most real materials contain grain boundaries and other preferential nucleation sites that are extremely important to the transformation kinetics

* See : J. W. Christian "The Theory of Phase Transformations in Metals and Alloys," 1981.

Analytical models have been developed for heterogeneously nucleated phase transformations

Microstructural Effects (J. W. Cahn, Acta. Metall., 1956)

$$X = 1 - \exp\left[-b^{-1/3} f(a)\right]$$

Grain boundary surface nucleation relationship

where:

$$f(a) = a \int_0^1 \left\{ 1 - \exp\left[-\pi a^3 \left(\frac{1-x^3}{3} - x^2(1-x) \right) \right] \right\} dx$$

$$S = \frac{3.35}{D}$$

$$a = t\left[IG^2 \right]^{1/3}$$

$$b = \frac{I}{8S^3 G}$$

Variables

- X : fraction transformed
- I(T) : nucleation rate
- G(T) : growth rate
- D : grain size

Assumptions

- spherical particle growth
- constant growth rate
- isothermal conditions

Non-isothermal microstructural evolution in welds occurs in three principal stages

a) Transformation to the high-temperature phase ($\alpha \rightarrow \beta$)
b) Rapid grain growth (single-phase β)
c) Transformation to the low-temperature phase ($\beta \rightarrow \alpha$)
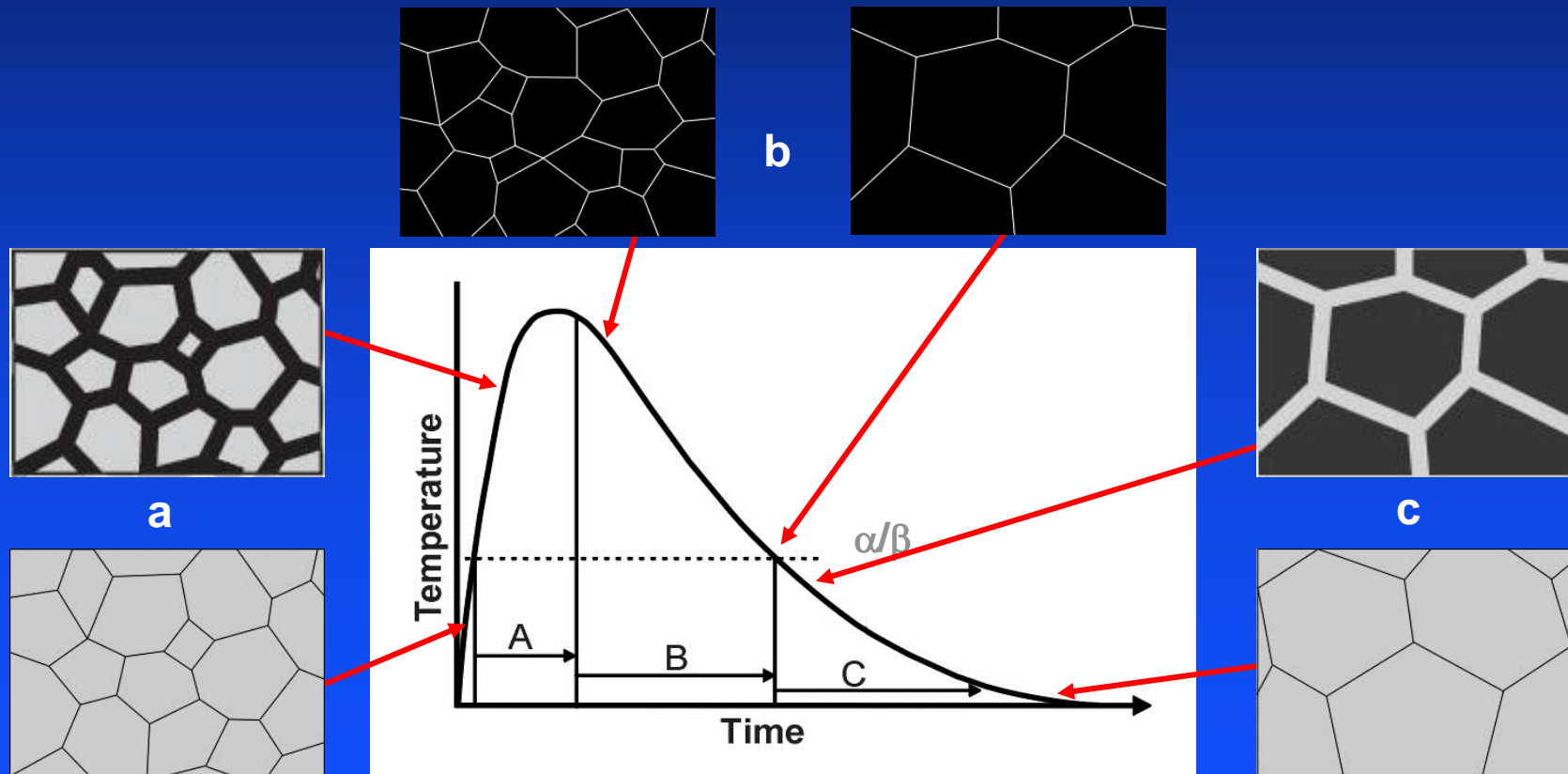
Generalized numerical weld HAZ phase transformations

Transformation to the high-temperature phase

start

$t = 0$
$T = T_{trans}$
$X = X_0$

Calculate:
$I(T), G(T), D(T)$

$$\frac{dX(I,G,D,t)}{dt}$$

Calculate: $T(t)$

$$X_{new} = X_{old} + \frac{dX}{dt}\Delta t$$

$t = t + \Delta t$ ← **No** — $T < T_{trans}$? ← **No** — $X_{new} = 1?$

Yes ↓ (below $T < T_{trans}$?)   **Yes** ↓ (below $X_{new} = 1?$)

Cooling kinetics

Grain Growth

finish
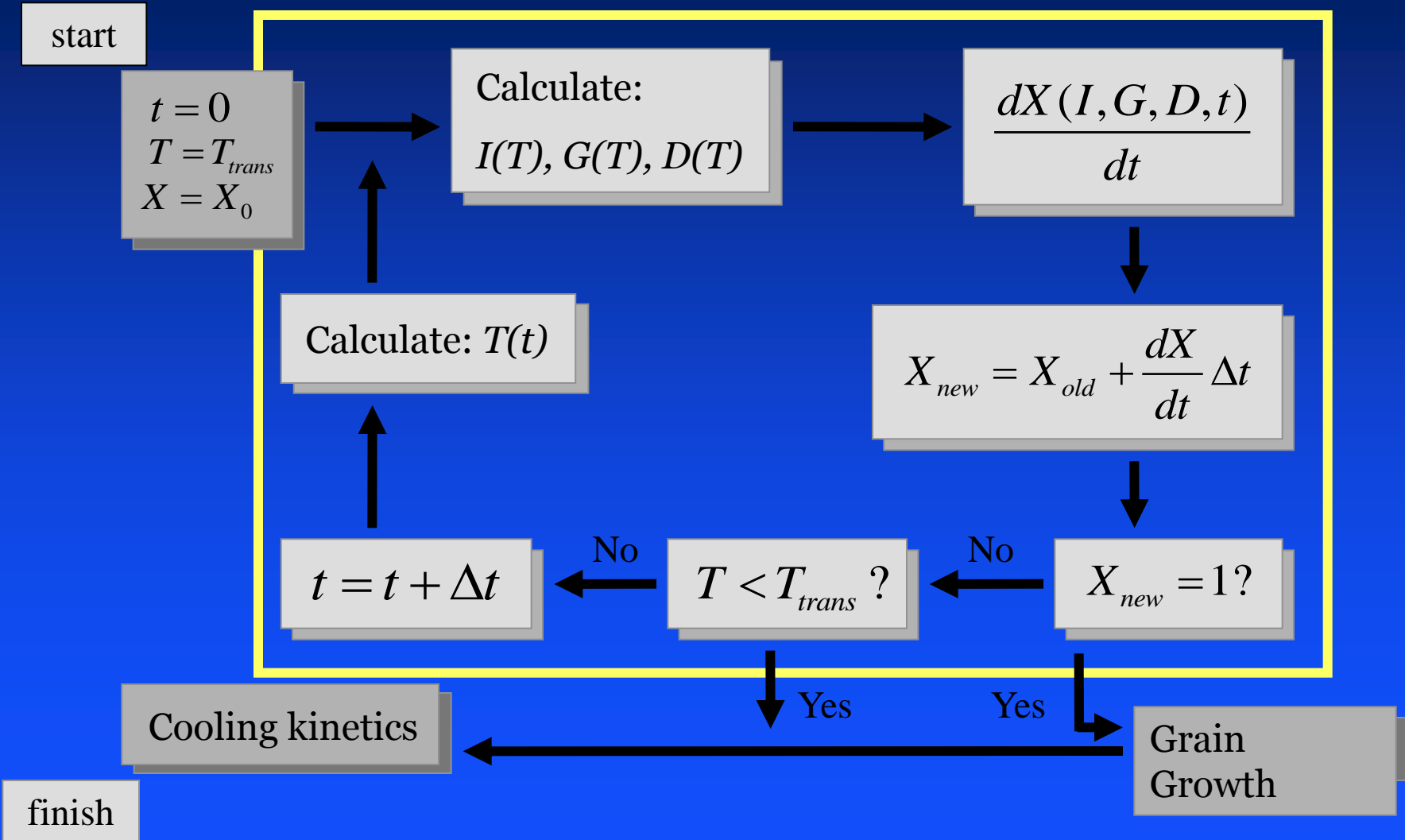
After transformation to the high temp phase, Monte Carlo approaches are used to calculate grain growth

Thermo-fluid model

SRXRD and
Previous JMA analysis

Microstructure

Weld thermal cycles

Grain growth
Kinetic parameters

Start temperature of growth

Monte Carlo model

γ grain distribution
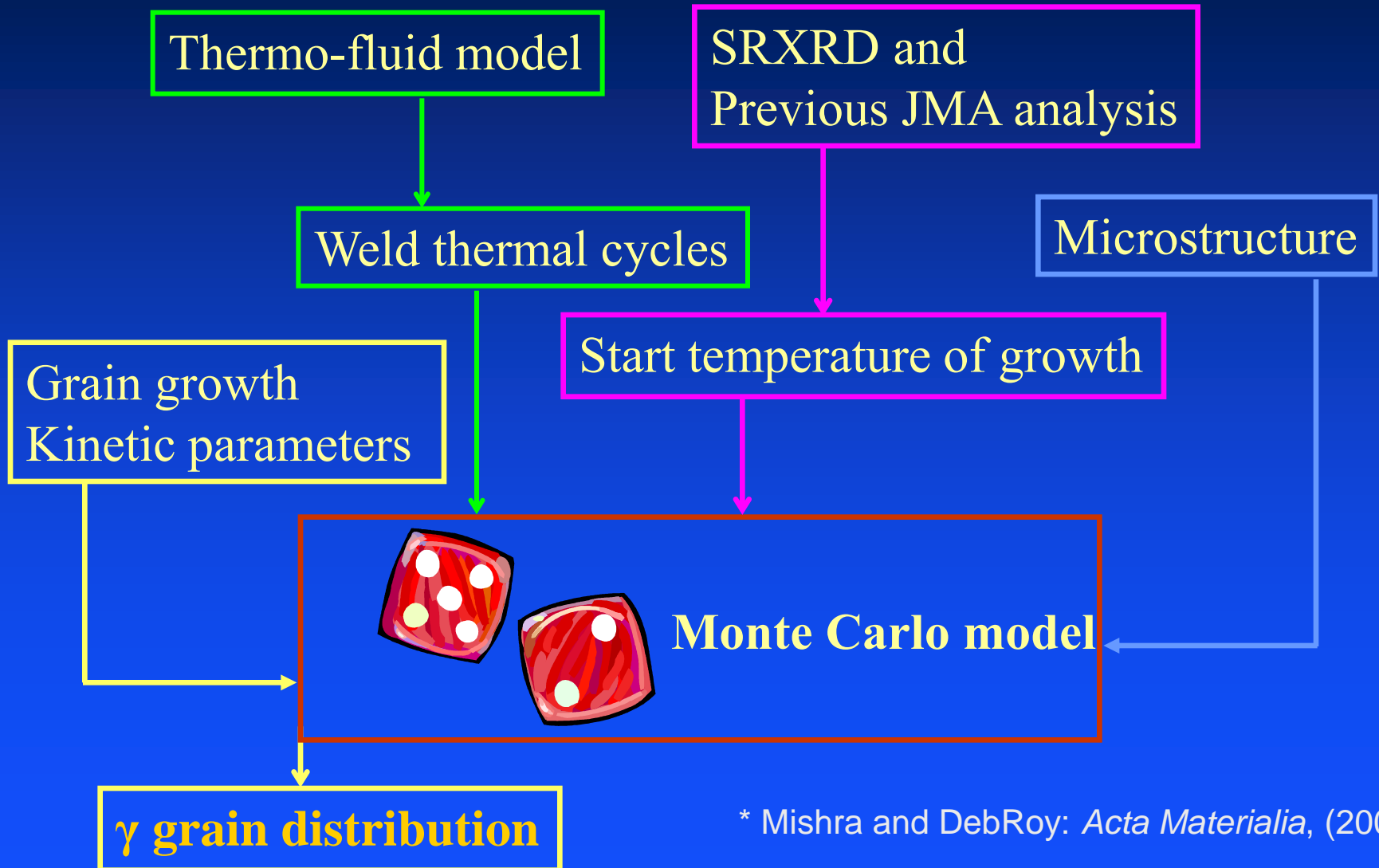
* Mishra and DebRoy: *Acta Materialia*, (2004)

Monte Carlo grain growth calculations in temp. gradeients and non-isothermal cond. are required

Monte Carlo Simulations of phase transformations in welds need to be coupled closely with experimental data for verification
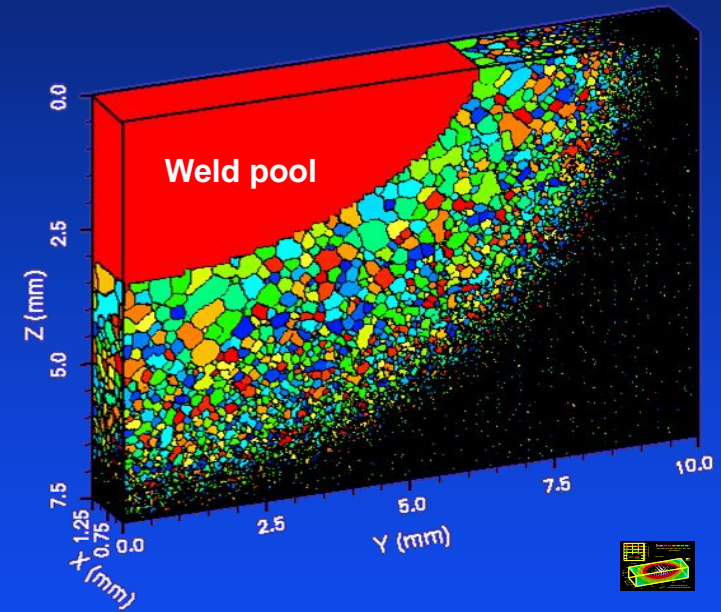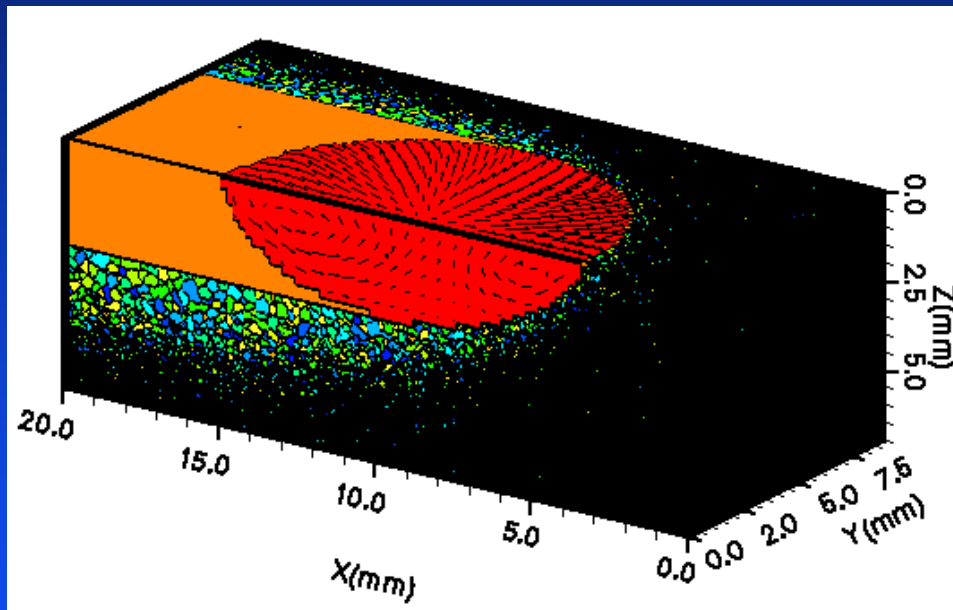
Numerical model of weld fusion zone, temperature profiles, and grain growth in the heat affected zone (HAZ) of titanium welds.

Z. Yang, S. Sista, J. W. Elmer, and T. DebRoy,"Three Dimensional Monte Carlo Simulation of Grain Growth During GTA Welding of Titanium," Acta Metall. Mater, 48 (12), pp. 4813-4825, 2000.

Part II
Time Resolved X-Ray Diffraction (TRXRD)
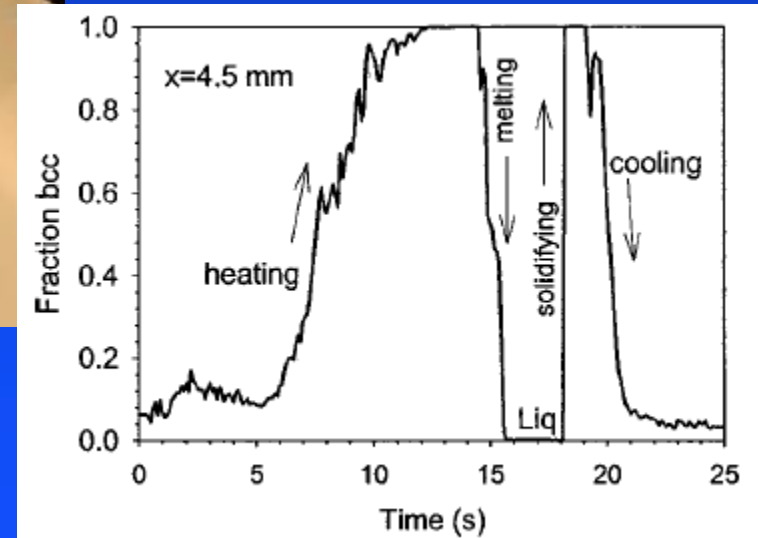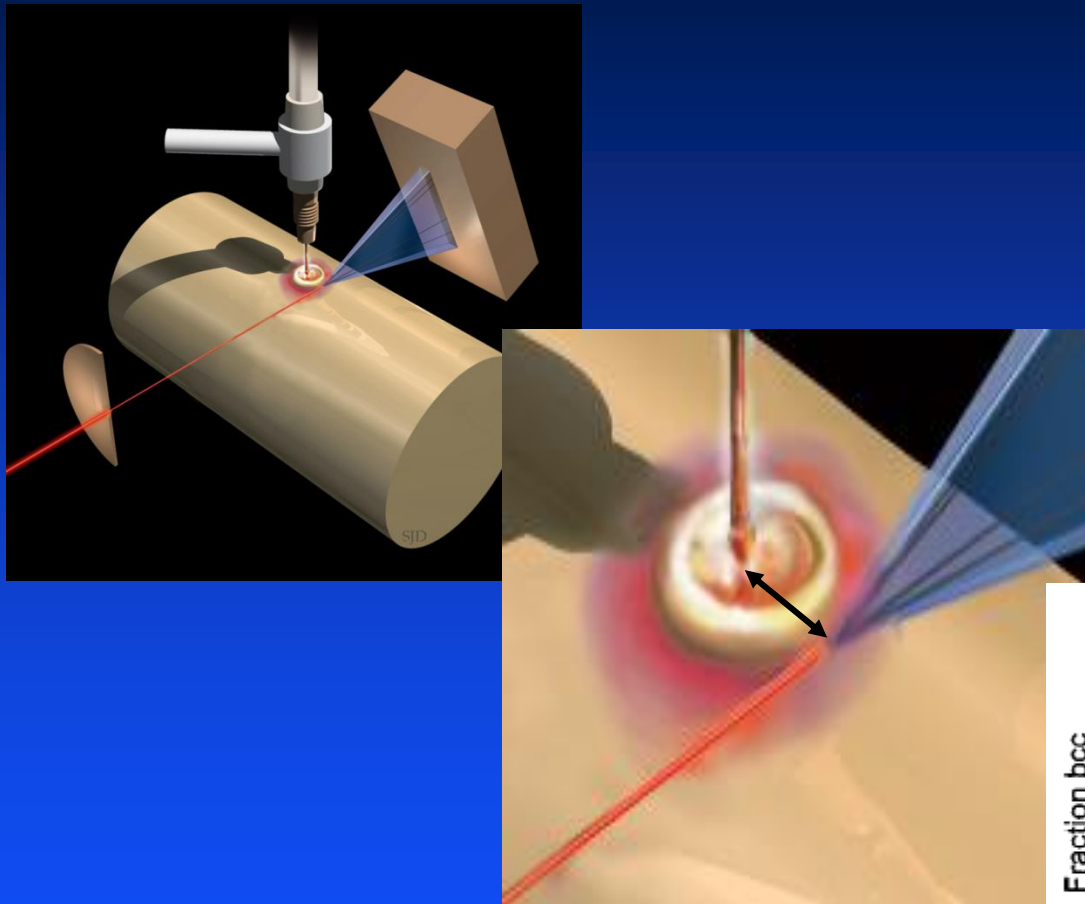
Phase transformation dynamics in Ti-6-4 weld, as tracked by TRXRD

Stationary "spot" welds allow us to look at much higher cooling rates than possible in moving welds

The arc is on for a short time then extinguished. The base metal extracts heat rapidly from the weld, which solidifies quickly

Thermocouple plunge experiments showed that the initial weld cooling rates can exceed 1000 K/s
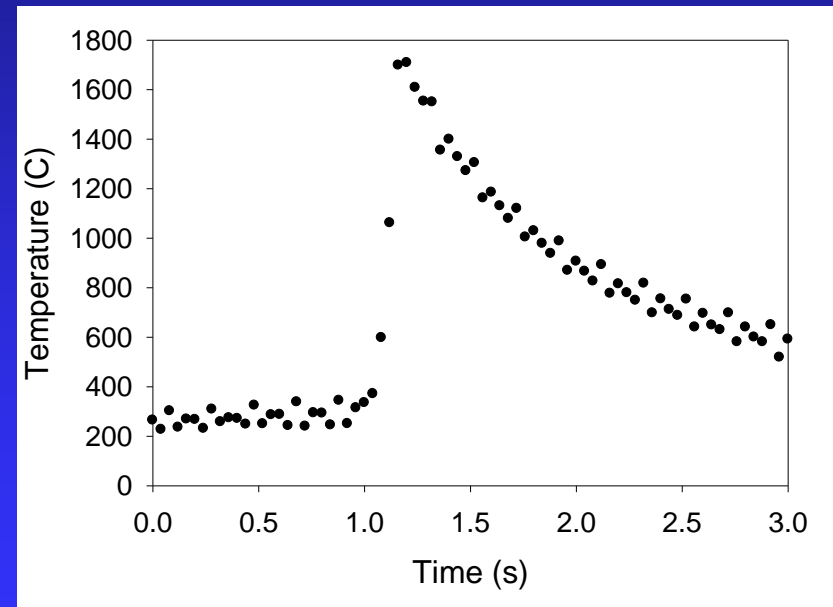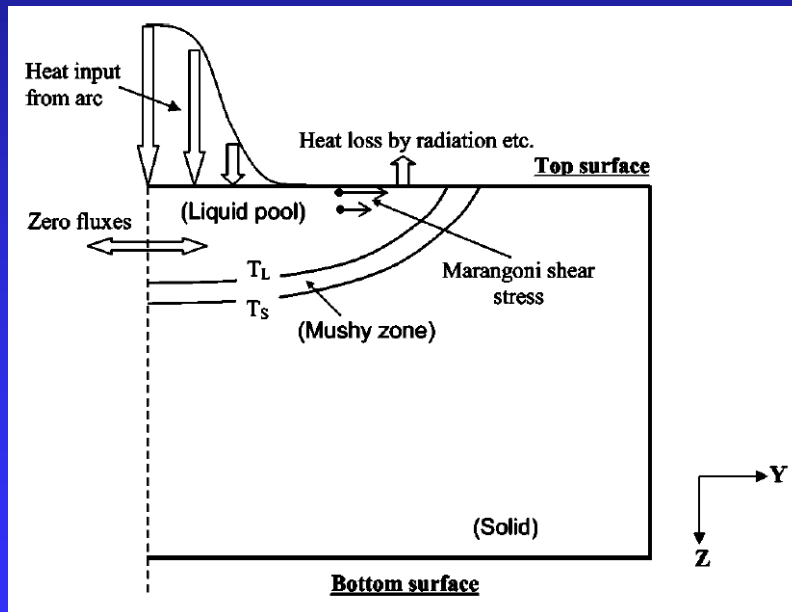
Transient temperature profiles require a 3D coupled thermal fluids computational approach

A 3D transient thermal-fluids weld model was developed at PSU for analyzing TRXRD results

Considerable computational effort is required to solve each transient spot weld problem. More than 10x the computational time is required for spot welds than for moving welds
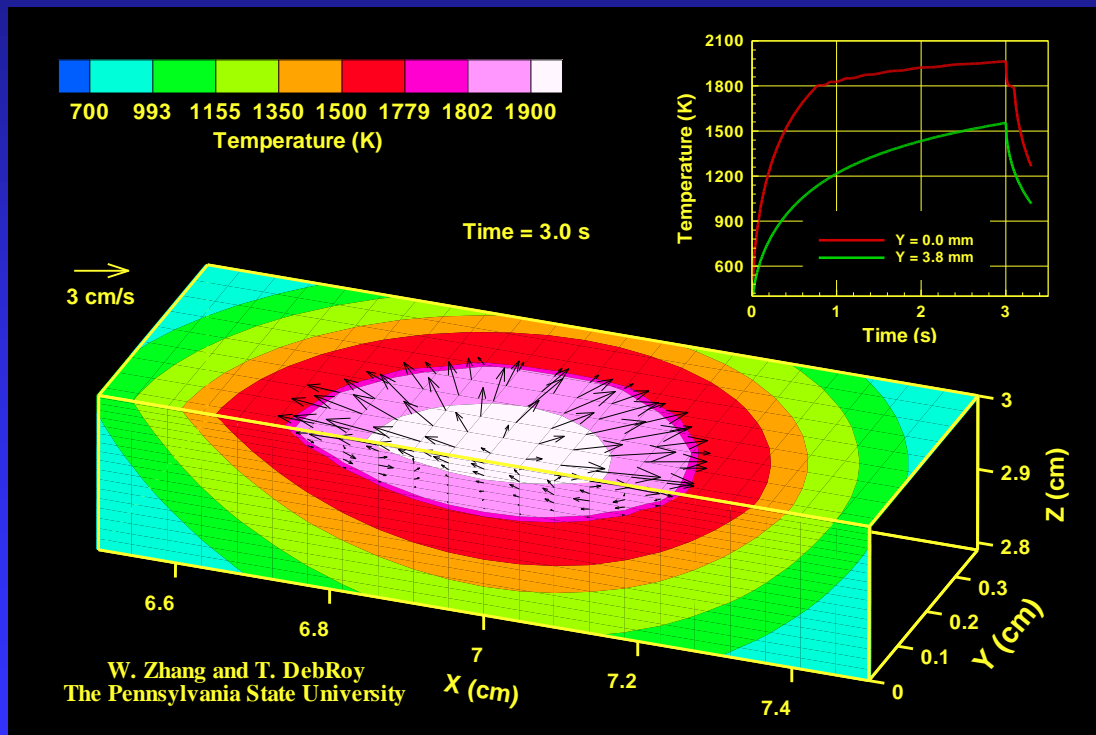
Calculated vs actual weld diameter 1005 Steel
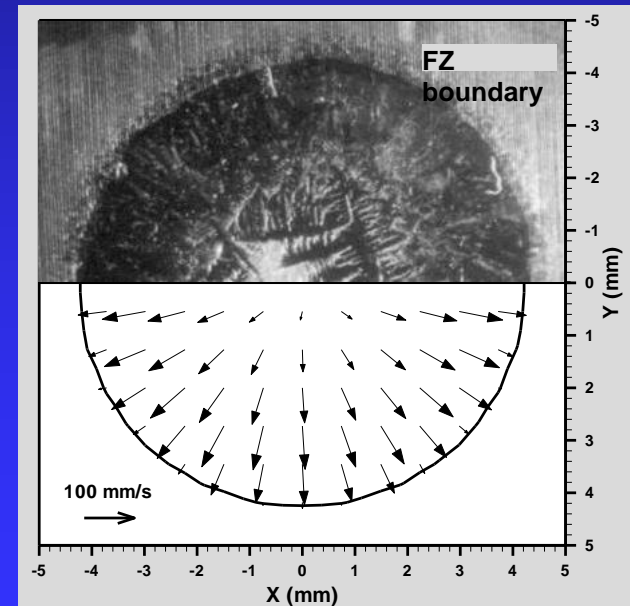
Martensite formation was directly observed using TRXRD during rapid cooling of 1045 steel

X-ray location in the HAZ
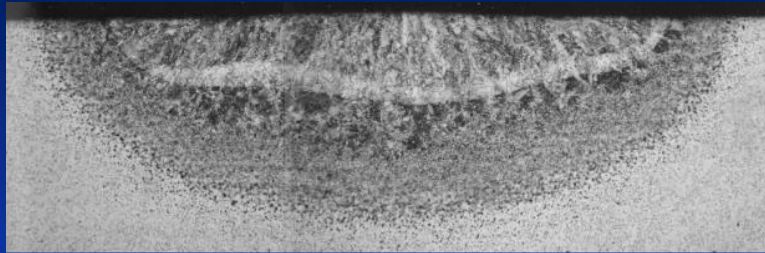
TRXRD at 100 ms/ frame

Rapid line broadening in 1045 steel during cooling indicates martensite formation
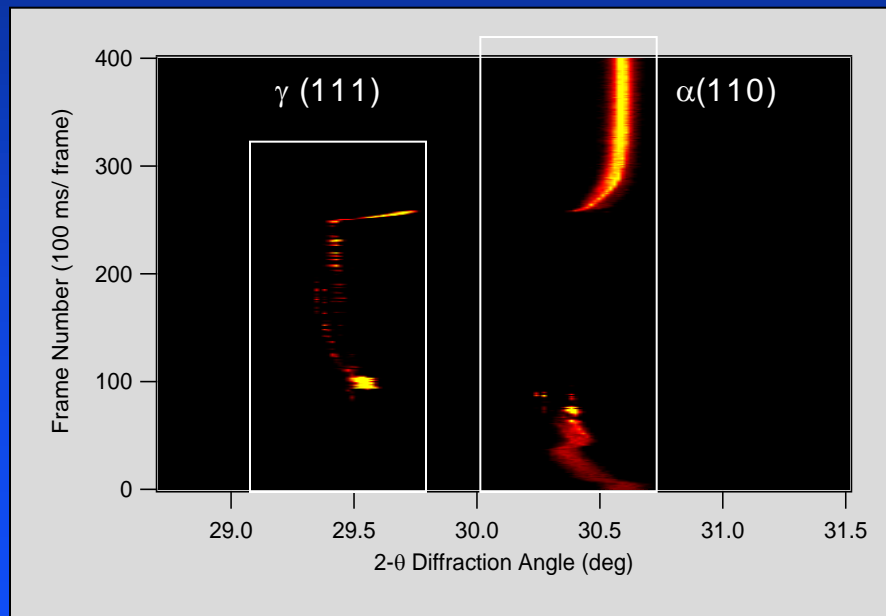
1005 Steel, 0.05% carbon no martensite formation
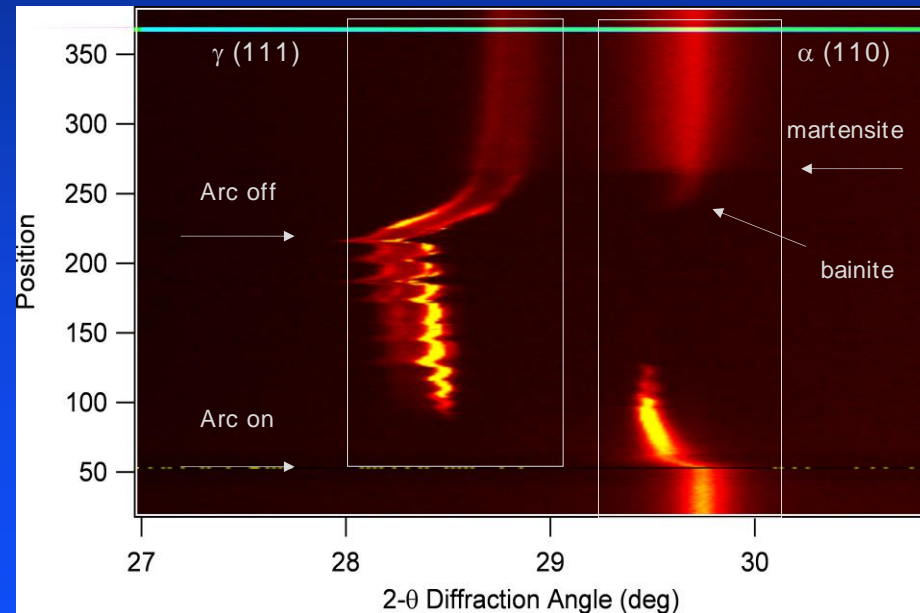
1045 Steel, 0.45% carbon martensite formation

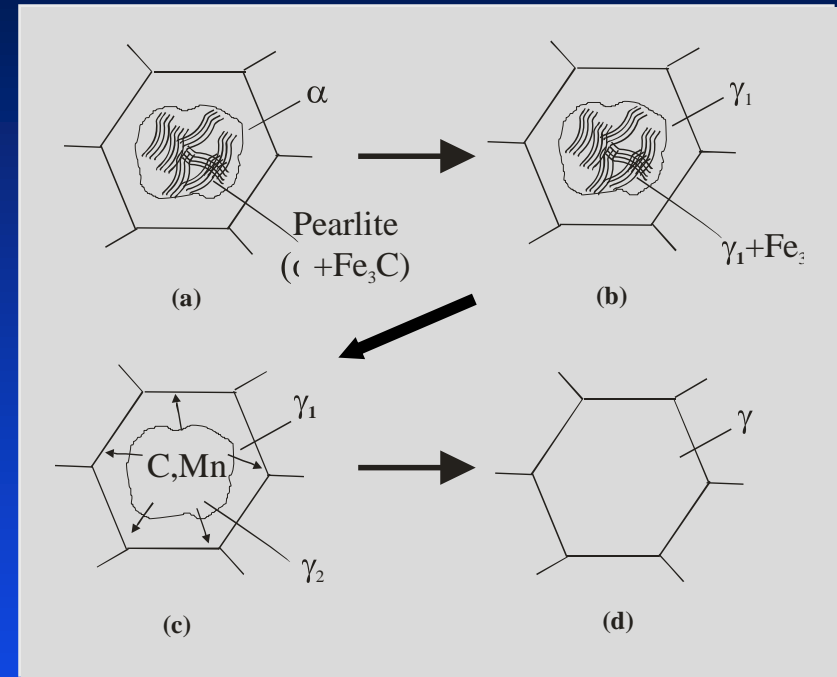# *Peak splitting in the austenite (γ phase) in the 1045 steel weld HAZs, shows two part transformation*

AISI 1045 Steel
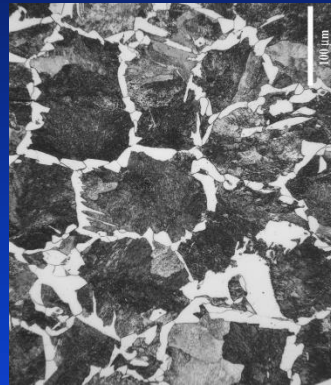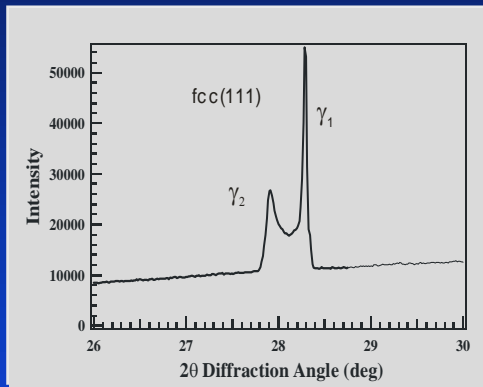
Diffraction pattern taken in the weld HAZ showing splitting of the fcc(111) austenite peak.

**The low 2θ peak builds from the existing high 2θ peak as the temperature increases**

Schematic diagram showing the progression of the $\alpha \rightarrow \gamma$ transformation and homogenization of the austenite.
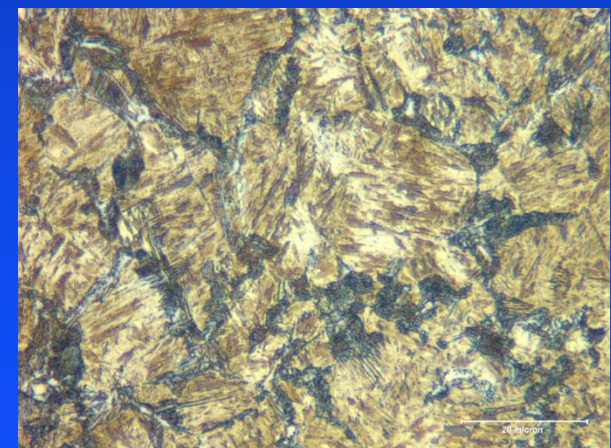
Arrows indicate increasing temperature

Analysis of the 1045 steel TRXRD data showed the transition from bainite to martensite during cooling

Lattice parameter and fraction bcc phase during the $\gamma \rightarrow \alpha$ phase transformation during cooling
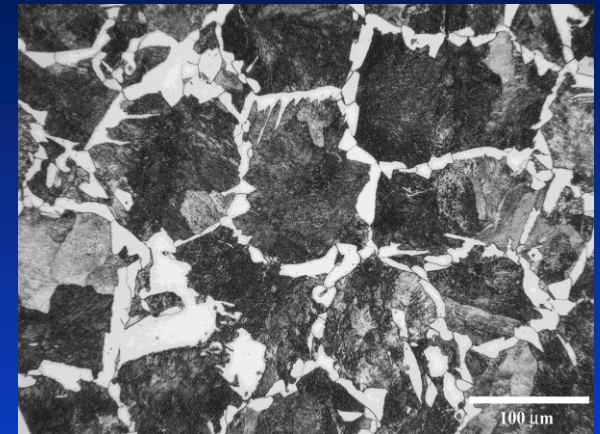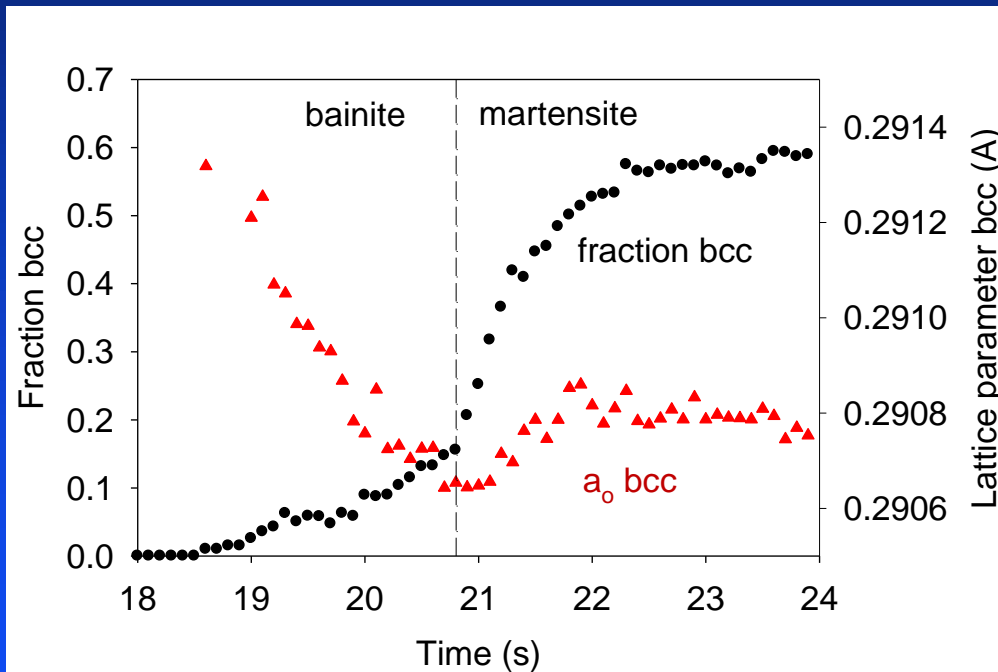
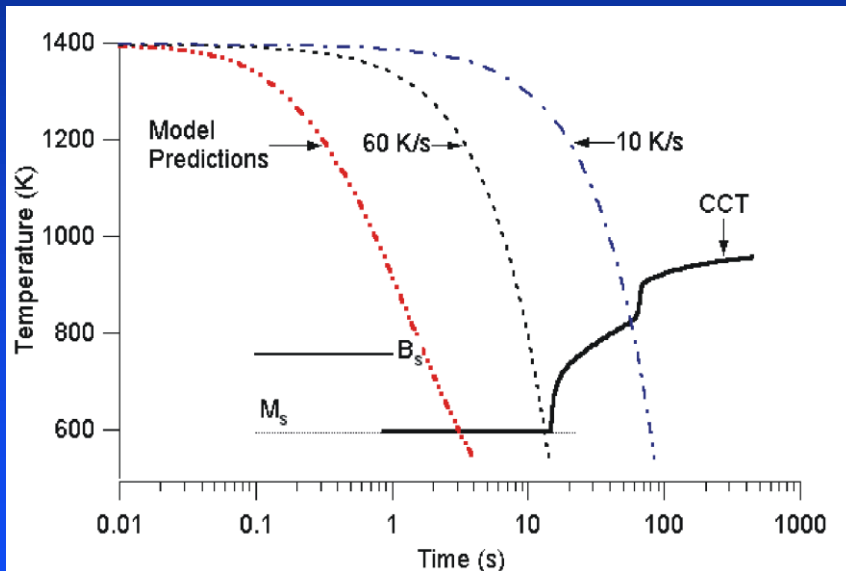**Before welding**

After welding

J. W. Elmer, T. A. Palmer, S. S. Babu, W. Zhang and T. Debroy, "Direct Observations of Austenite, Bainite, and Martensite Formation During Arc Welding of 1045 Steel using Time Resolved X-ray Diffraction," Welding Journal, V83(9), pp 244-s to 253-s, 2004.

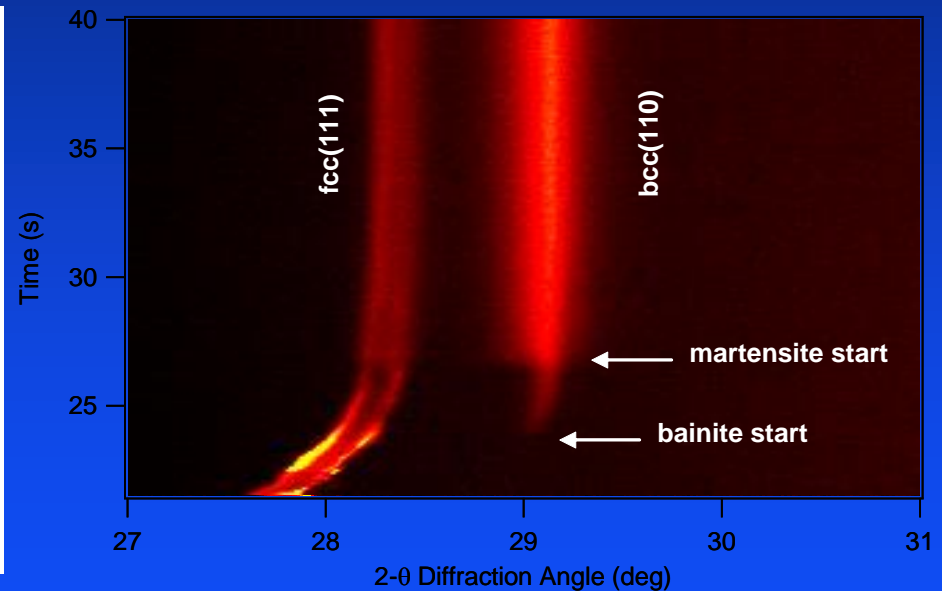# *Microstructural modeling of the 1045 steel predicts bainite followed by martensite for the TRXRD exp*

The calculated CCT diagram shows that the $\gamma \rightarrow \alpha$ transformation should start via a bainitic reaction and finish via a martensitc reaction at cooling rates higher than 60C/s.

CCT diagram for 1045 steel

TRXRD confirmation

J. W. Elmer, T. A. Palmer, S. S. Babu, W. Zhang and T. Debroy, "Direct Observations of Austenite, Bainite, and Martensite Formation During Arc Welding of 1045 Steel using Time Resolved X-ray Diffraction," Welding Journal, V83(9), pp 244-s to 253-s, 2004.

Comparison between the 1005 and 1045 steels shows the effects of microstructure on $\alpha \rightarrow \gamma$ *kinetics*
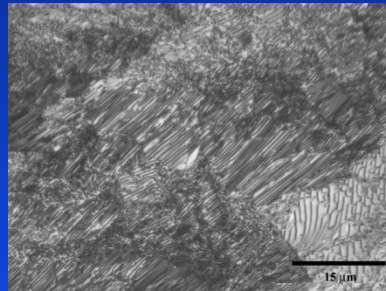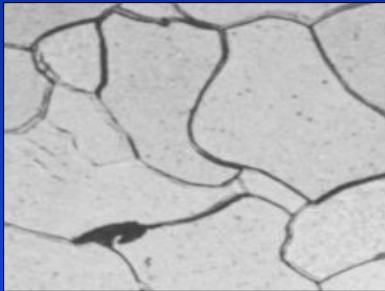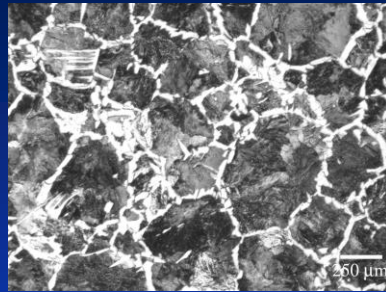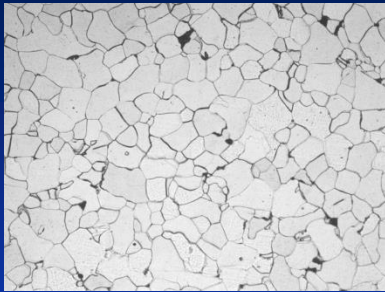
1005 Steel,
0.05% carbon
20μm grain size
small amount of pearlite

1045 Steel,
0.45% carbon
90 μm grain size
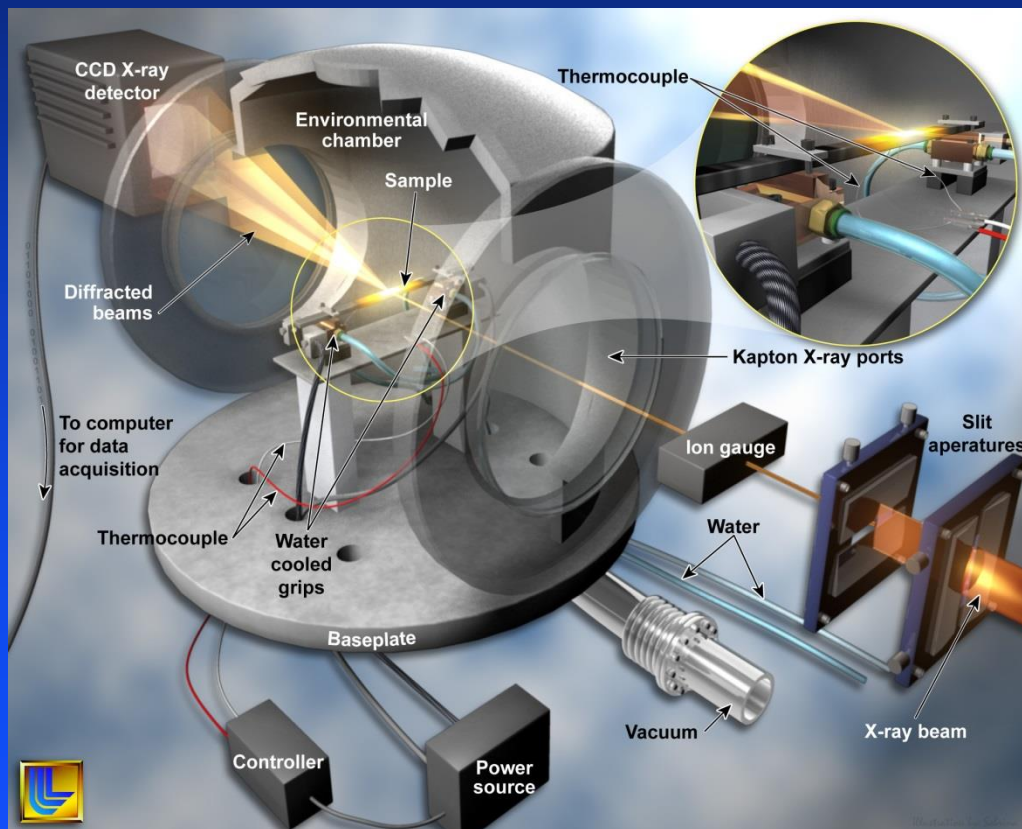**high fraction pearlite**
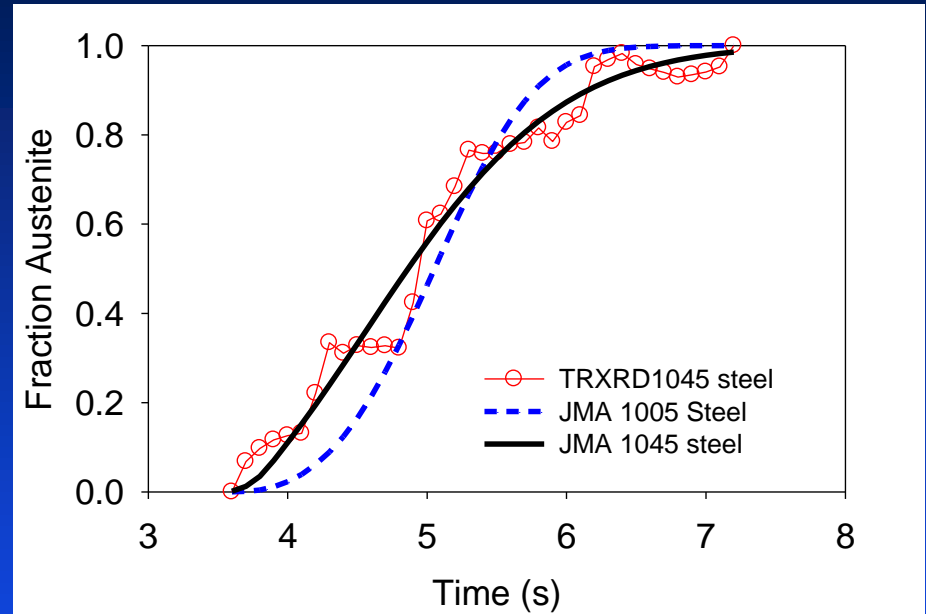
High nucleation rate in the 1045 steel causes initial high transformation rate

Larger grain size of the 1045 steel results in longer total time to complete the transformation

Part III
Controlled Heating and Cooling Experiments
at the Advanced Photon Source

In-situ experiments are performed at APS inside an environmental chamber

- UNICAT BM-33-C
- 30 keV beam
- 1 mm x 0.25 mm beam
- 10^{-4} torr
- 1024 x 1024 CCD
- 1s integration time
- water cooled grips
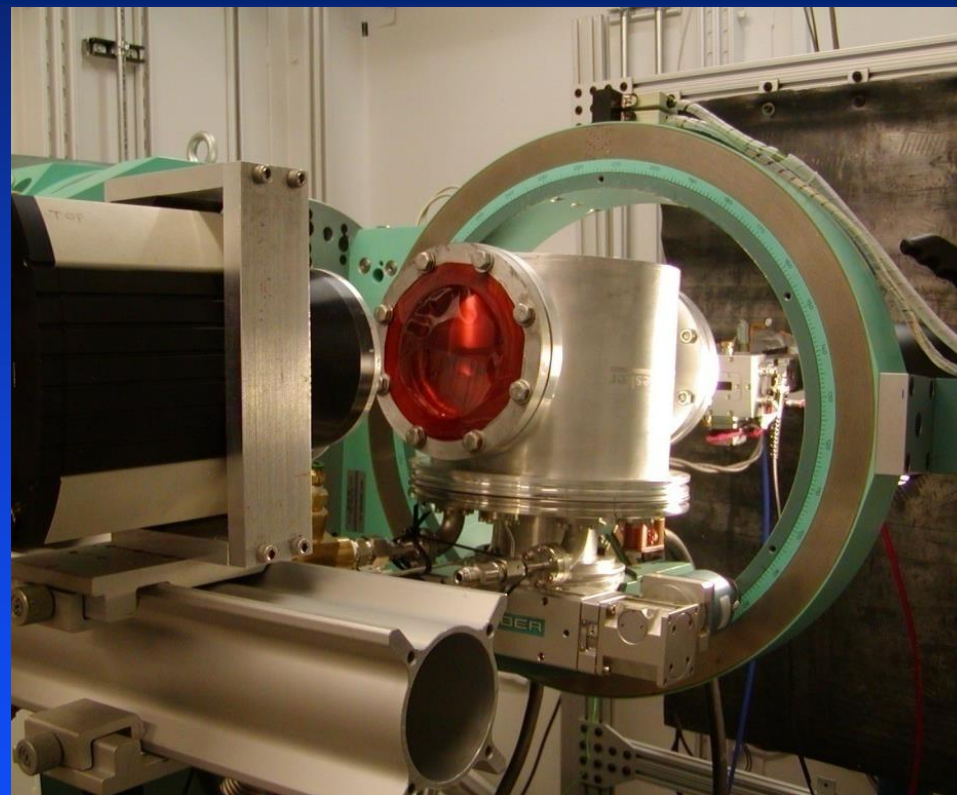- ~20C/s heat/cool rate

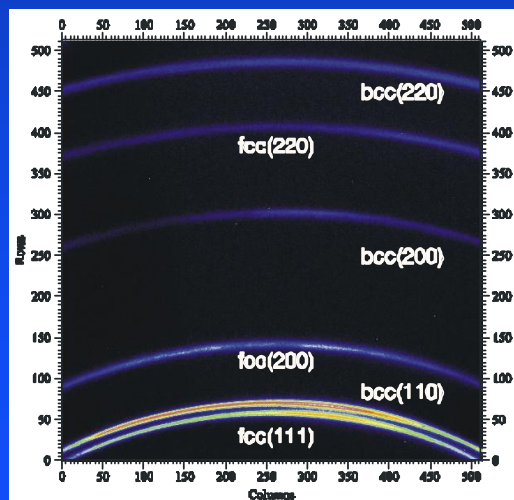# Controlled heating experiments provide more control over temperature than in-situ welding experiments

Any heating/cooling profile can be programmed into the heating system.
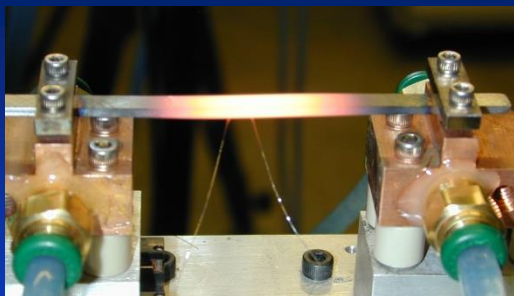
Sample being heated in water cooled copper grips

Areal detector

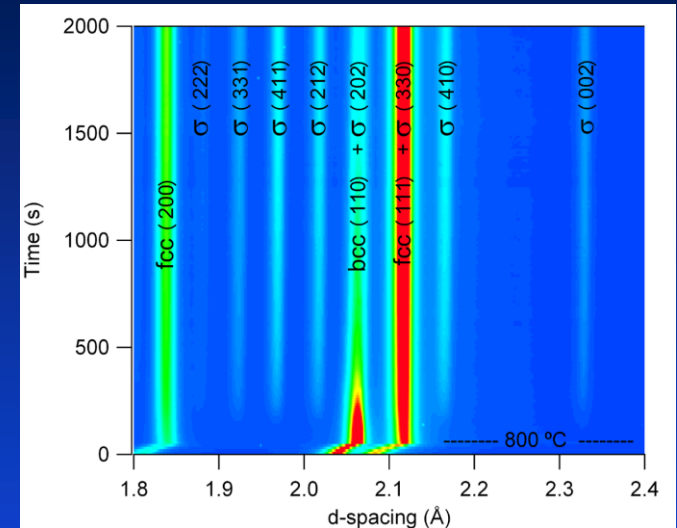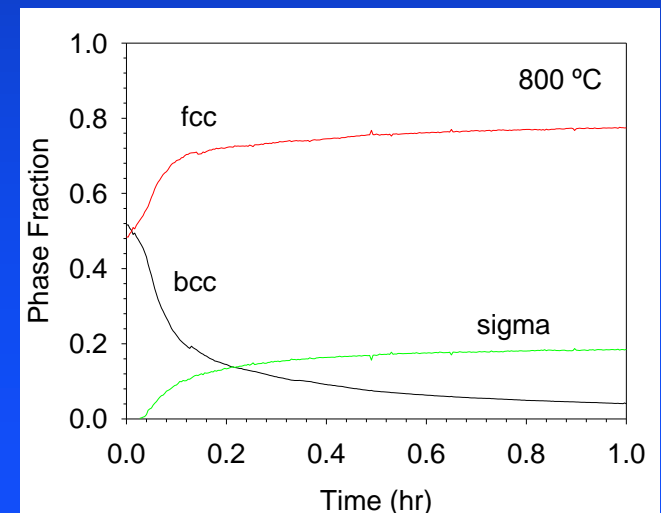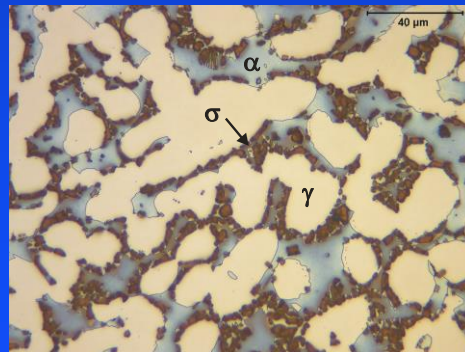Goniometer stage at the APS with environmental chamber in place

Example 1: Sigma phase formations in 2205 duplex stainless steel (DSS)

The formation and growth of sigma (σ) phase in 2205 DSS was monitored in real time using synchrotron radiation at temperatures between 700^{0}C and 850°C, where transformation to σ is rapid. The synchrotron data at the right shows that σ forms as ferrite decomposes to a combination of sigma plus austenite. Other results show the dissolution of σ at higher temperatures close to 1000°C. The kinetics of sigma formation were modeled using the JMAK approach to determine predictive capability for sigma formation.

Final microstructure
After 800°C run showing
sigma formation

J. W. Elmer, T. A. Palmer and E. D. Specht, "Direct Observations of Sigma Phase Formation in Duplex Stainless Steels Using In-Situ Synchrotron X-Ray Diffraction," Metallurgical and Materials Transactions A, 38A(3), pp464-475, 2007
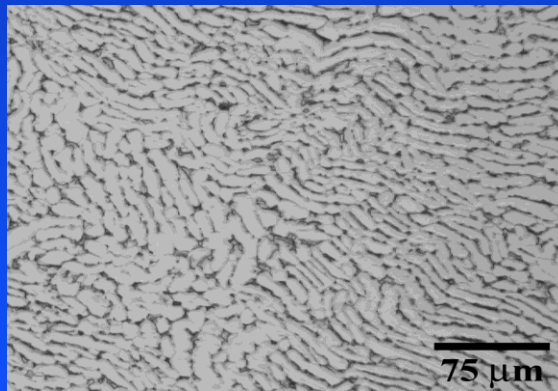
Example 2: phase transformations, selective vanadium partitioning and stress relaxation in Ti-6-4
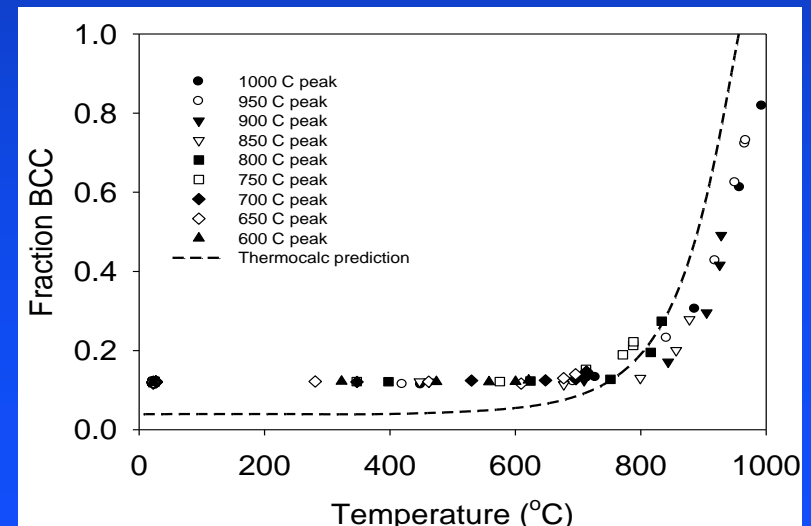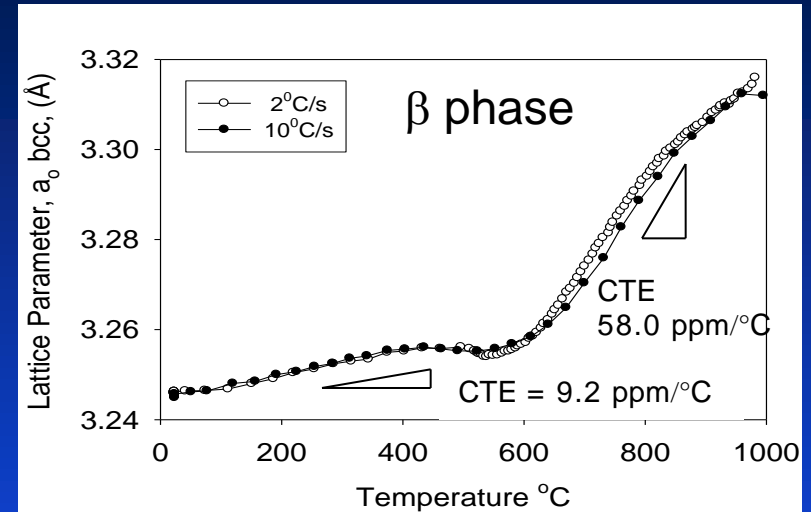
Ti-6Al-4V contains α and β phases at room temperature and the phase ratio changes with temperature. In situ synchrotron measurements measured 1) α/β ratio, 2) lattice parameter of α and β phases at different rates.

- Annealing begins at 550ºC
- Phase transformation begins at 750ºC
- CTE of β increases 5x during trans. due to selective partitioning of V

Ti-6-4 starting microstructure

J. W. Elmer, T. A. Palmer, S. S. Babu, and E. D. Specht, "In-situ Observations of Lattice Expansion and Transformation Rates of a and b Phases in Ti-6Al-4V," Materials Science and Engineering A, 391, pp104-113, January, 2005.

Example 3: Measuring diffusion coefficients, gold/copper interdiffusion for microelectronics
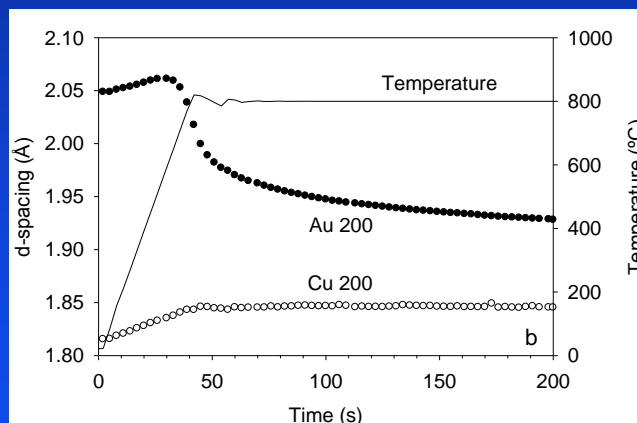
In-situ x-ray diffraction performed on thin-film Au/Cu binary diffusion couples directly observed diffusion at temp. from 700ºC to 900ºC. The activation energy for interdiffusion was measured to be 65.4 kJ/mole, which is approximately 0.4x that for bulk diffusion and 0.8x that for grain boundary diffusion. The low activation energy is attributed to the high density of columnar grain boundaries combined with other defects in the sputter deposited thin film coatings.
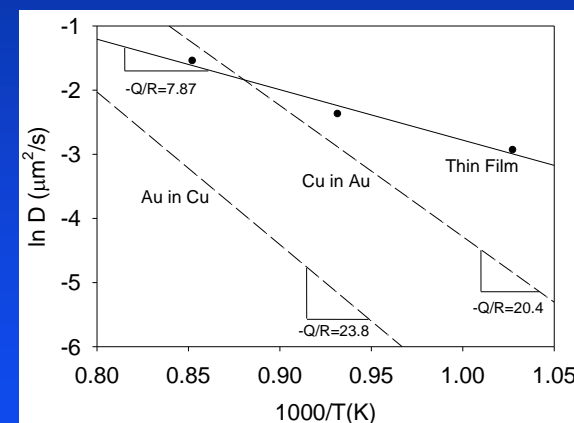

25 mm

Sample showing PVD layers of 3.8 μm Au over 35 μm Cu layer on SS
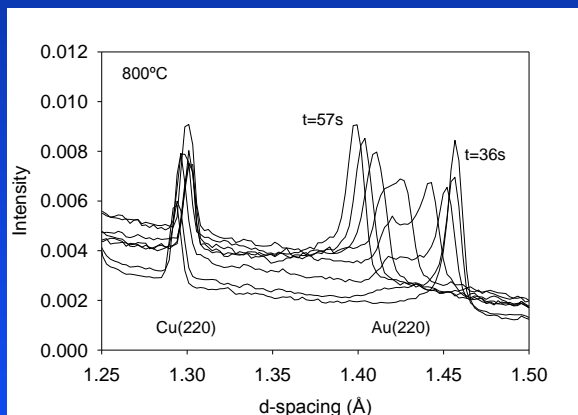
Au and Cu 220 peaks at 800°C at 3s intervals

Lattice parameter for Au and Cu at 800°C

Low measured activation energy for thin films

J. W. Elmer, T. A. Palmer and E. D. Specht, "Direct Observations of Rapid Diffusion of Cu in Au Thin Films using In-Situ X-Ray Diffraction," Journal of Vacuum Science and Technology-A, 24(4) July/Aug, pp. 978-987, 2006.

Example 4: Microstructure development in DP600 steel using synchrotron data and Phase Field Modeling: Dr Richard Thiessen, Technical University of Delft
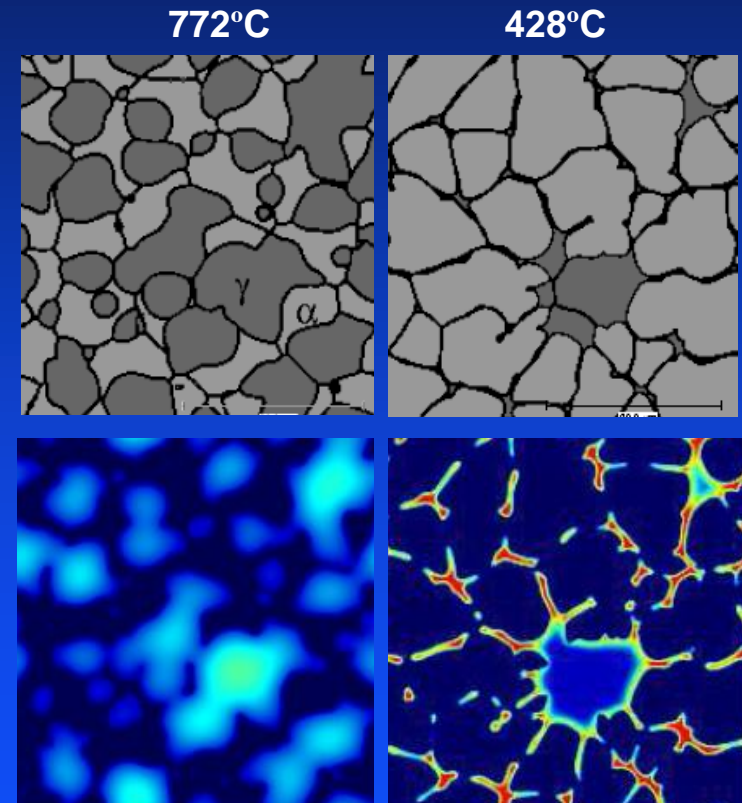
Dual phase steels undergo martensitic phase transformations on cooling, creating a mixture of martensite, ferrite and small amounts of residual austenite. When properly heat treated high strengths with enhanced ductility steels are created. In-situ synchrotron studies monitored phase transformations of DP600 both on heating and cooling to verify phase field models of these transformations.
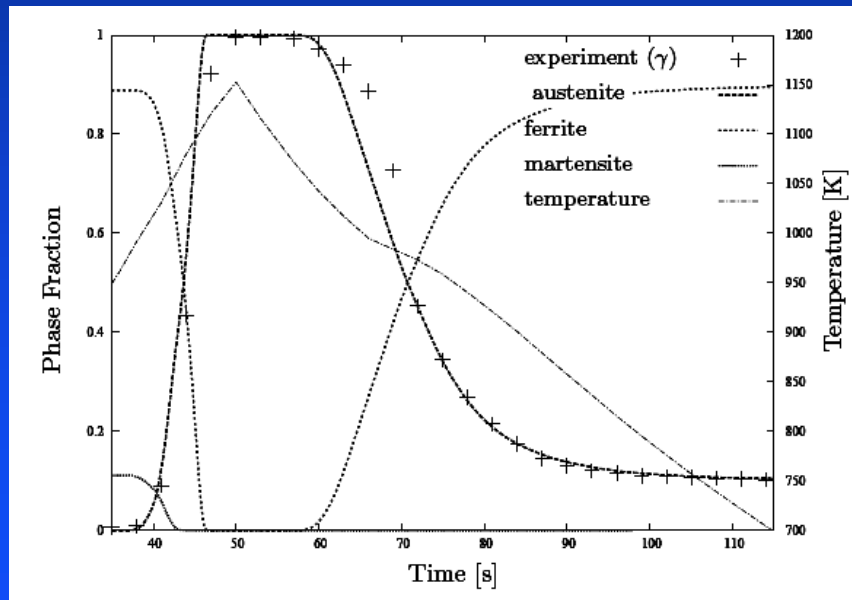
Comparison of synchrotron experimental data (+ symbols), with phase field calculations (lines)

Phase field calculations: micro-structure (top) and carbon distribution (bottom)

772°C   428°C

R. G. Thiessen, J. Sietsma, T. A. Palmer, J. W. Elmer and I. M. Richardson,"Phase-Field Modelling and Synchrotron Validation of Phase Transformations in Martensitic Dual-Phase Steel," Acta Materialia, 55, pp. 601-614, 2007.
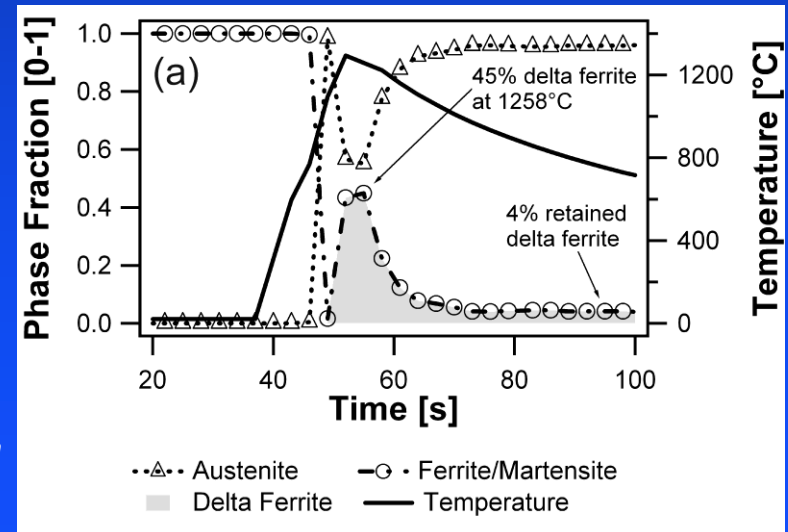
Example 5: Microstructure development in a boron alloyed 9Cr-3W-3Co-V-Nb steel for power plants: Dr. Peter Mayr, Technical University, Graz, Austria

Martensitic 9-12 wt.% chromium steels with controlled additions of boron and nitrogen are processed by complex heat treatment, to create a fully martensitic microstructure with finely dispersed precipitates, but retention of delta ferrite reduces properties. Here Synchrotron experiments were performed to simulate thermal cycles typical of welding and post-weld heat treating to observe the formation and retention of delta ferrite.
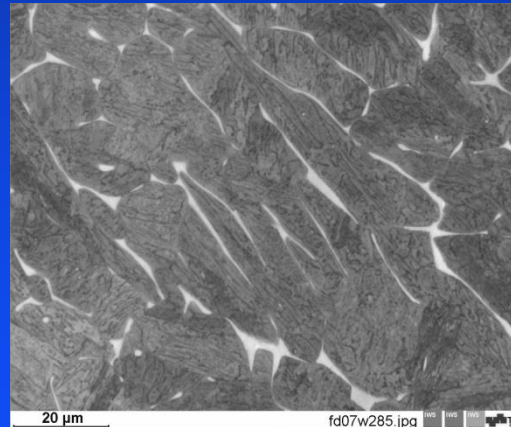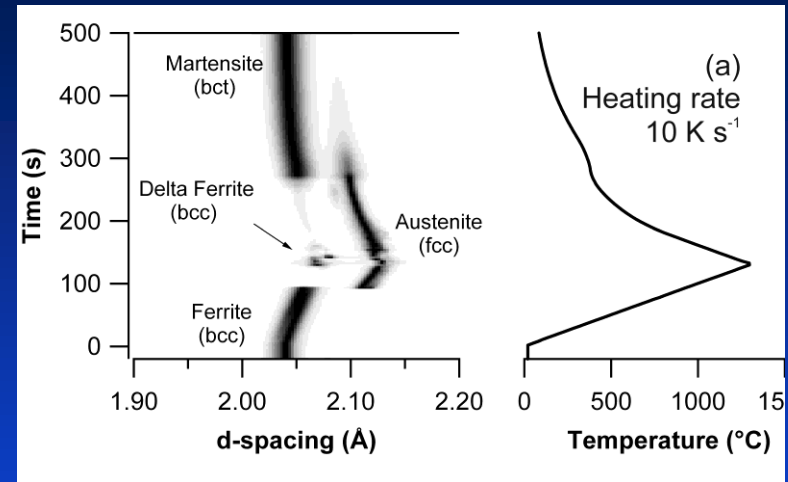
Final microstructure after 100°C/s heat rate. Residual delta ferrite etches light in color

P. Mayr, T. A. Palmer, J. W. Elmer, E. D. Specht, and S. M. Allen, "Formation of Delta Ferrite in 9 wt% Cr Steel Investigated by In-Situ X-ray Diffraction Using Synchrotron Radiation," Metallurgical and Materials Transactions A, 41A (10), pp. 2462-2465, 2010.

Summary: In-situ synchrotron studies provide unique information that can help verify numerical models of phase transformations in metals and alloys

Conventional weld characterizatin methods are indirect or ex-situ

- **Dilatometry / Gleeble testing**
- **Electrical Resistivity**
- **Differential Scanning Calorimetry**
- **Post Weld Metallography**
- **Isothermal hold, quench and inspection**

In-Situ synchrotron experiments for weld model verification

- **Provides real time observations of transformations as they occur**
- **Allows microstructural evolution to be observed in real time**
- **Can be used to gather kinetic data for verification of weld models under high and low cooling rates**
    - **Crystal structure change on heating, melting, solidification and cooling up to the melting point of any metal or alloy**
    - **Phase transformation kinetics**
    - **Diffusion coefficient measurements**
    - **Grain growth and refinement**
    - **Lattice parameter measurements**
    - **Coefficient of thermal expansion, phase and orientation dependent**

Acknowledgement